11-1-2017

Computational Prediction of Conductivities of Disk-Shaped Particulate Composites

Jian Qiu
University of Denver

Computational Prediction of Conductivities of Disk-Shaped Particulate Composites

Abstract

The effective conductivities are determined for randomly oriented disk-shaped particles using an efficient computational algorithm based on the finite element method. The pairwise intersection criteria of disks are developed using a set of vector operations. An element partition scheme has been implemented to connect the elements on different disks across the lines of intersection. The computed conductivity is expressed as a function of the density and the size of the circular disks or elliptical plates. It is further expressed in a power-law form with the key parameters determined from curve fittings. The particle number and the trial number of simulations vary with the disk size to minimize the computational effort in search of the percolation paths. The estimated percolation threshold agrees well with the result reported in the literature. It has been confirmed that the statistical invariant for percolation is a cubic function of the characteristic size, and that the definition of percolation threshold is consistent with that of the equivalent system containing spherical particles. The effect of aspect ratio to the percolation threshold has been studied in this article. High aspect ratio will decrease the percolation threshold. Binary dispersions of disks of different radii have also been investigated to study the effect of the size distribution. The approximate solutions in the power-law function have potential applications in advanced composites with embedded graphene nanoplatelets.

Document Type

Thesis

Degree Name

M.S.

Department

Materials Science

First Advisor

Yun-Bo Yi, Ph.D.

Second Advisor

Matthew Gordon

Third Advisor

Chadd Clary

Keywords

Conductivity, Disk-shaped particulate, Finite element analysis, Graphene nanoplatelets, Monte Carlo simulation, Simulation

Subject Categories

Materials Science and Engineering | Nanoscience and Nanotechnology

Computational Prediction of Conductivities of Disk-Shaped Particulate Composites

_____

A Thesis

Presented to

The Faculty of the Daniel Felix Ritchie School of Engineering and Computer Science

University of Denver

_____

In Partial Fulfillment

of the Requirements for the Degree

Master of Science

_____

by

Jian Qiu

August 2014

Advisor: Dr. Yun-Bo Yi

Author: Jian Qiu
Title: Computational Prediction of Conductivities of Disk-Shaped Particulate Composites
Advisor: Dr. Yun-Bo Yi
Degree Date: August 2014

ABSTRACT

The effective conductivities are determined for randomly oriented disk-shaped particles using an efficient computational algorithm based on the finite element method. The pairwise intersection criteria of disks are developed using a set of vector operations. An element partition scheme has been implemented to connect the elements on different disks across the lines of intersection. The computed conductivity is expressed as a function of the density and the size of the circular disks or elliptical plates. It is further expressed in a power-law form with the key parameters determined from curve fittings. The particle number and the trial number of simulations vary with the disk size to minimize the computational effort in search of the percolation paths. The estimated percolation threshold agrees well with the result reported in the literature. It has been confirmed that the statistical invariant for percolation is a cubic function of the characteristic size, and that the definition of percolation threshold is consistent with that of the equivalent system containing spherical particles. The effect of aspect ratio to the percolation threshold has been studied in this article. High aspect ratio will decrease the percolation threshold. Binary dispersions of disks of different radii have also been investigated to study the effect of the size distribution. The approximate solutions in the power-law function have potential applications in advanced composites with embedded graphene nanoplatelets.

ACKNOWLEDGMENTS

During my graduate study I have been working on computational simulation one year and I cannot stop thinking of its contribution to the Materials Science in the past years and the promising development in the future.

Also, I would like to thank my advisor Dr. Yi for his giving me this unique opportunity to work with computational simulation and for his support on all of my research. I still remember how I was excited when Dr. Yi assigned me this project; I remember the exciting moment when I finished an important part of the project. I also want to thank Dr. Xiaobo Guo at the University of Texas, Dallas who made a significant amount of efforts on the previous work. I also want to appreciate all my lab mates who gave me lots of courage and motivation to complete this research. Also many thanks to the University of Denver administrators and professors and staffs to have me here and let me study at DU. I have learned a great deal and I feel lucky to be a student at DU.

TABLE OF CONTENTS

LIST OF FIGURES

LIST OF TABLES

CHAPTER ONE: INTRODUCTION

1.1 Introduction of Graphene and Graphene-Based Composite

1.1.1 Graphene and graphene nano-platelets (GNP)

Graphene is a rapidly rising super star on the horizon of materials science and condensed matter physics. In spite of a short history, this purely two-dimensional material shows unconventionally high crystal and electronic quality, this will briefly be discussed here. Whereas one can be certain of the realness of applications only when commercial products appear, graphene no longer requires any further proof of its importance in terms of fundamental physics. Due to its unusual electronic spectrum, graphene has led to the emergence of a new paradigm of "relativistic" condensed matter physics, where quantum relativistic phenomena, some of which are unobservable in high energy physics, can now be mimicked and tested in table-top experiments. More generally, graphene represents a conceptually new class of materials that are only one atom thick and, on this basis, offers new inroads into low-dimensional physics that has never ceased to surprise and continues to provide a fertile ground for applications [1], [2].

Graphene is a flat monolayer of carbon atoms firmly packed into a two-dimensional (2D) honeycomb lattice, and is a basic structural element for all other dimensionalities graphitic materials. It can be wrapped up into 0D fullerenes, rolled into 1D nanotubes or stacked into 3D graphite. Figure 1.1 shows the graphene structure.

Figure 1.2 shows the graphene-based materials. Superior quality graphene is a strong, light, and nearly transparent crystal with remarkable heat and electrical performances. Graphene exhibits some unique properties, such as the ballistic transport of charges andlarge quantum oscillations and bipolar transistor [1], [2], [3]. Because of the promise of future applications in nanoelectronics, the prior research on graphene was primitively prompted by its peculiar electrical transport properties. However, graphene sheets, due to their particular thermal and mechanical properties and high electrical conductivity, are also of great interest to be treated as new nanoscale structural elements to create unique macroscopic composite materials [2], [3]. Graphene sheets, also called graphene nano-platelets (GNP), are disk-shaped nanoparticles which consist of 10-100 layers of graphene produced through exfoliation [4]. Figure 1.3 shows the diameters of the plates ranging from sub-micrometer to 100 micrometers. Because of its unique size and morphology, graphite nano-platelet can be combined with other polymer materials (plastic, nylon, or rubbers) to enhance mechanical properties and thermal conductivity due to their pure graphitic composition [5], [6].

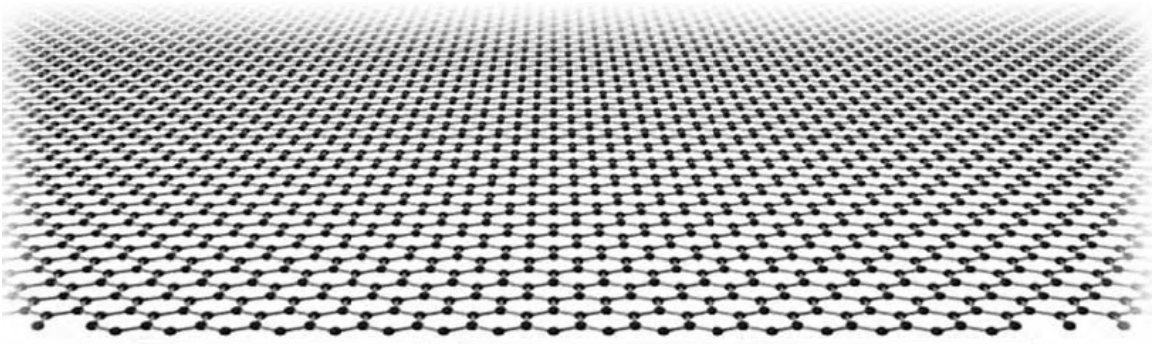

Figure 1.1: Graphene structure: a 2D honeycomb material.

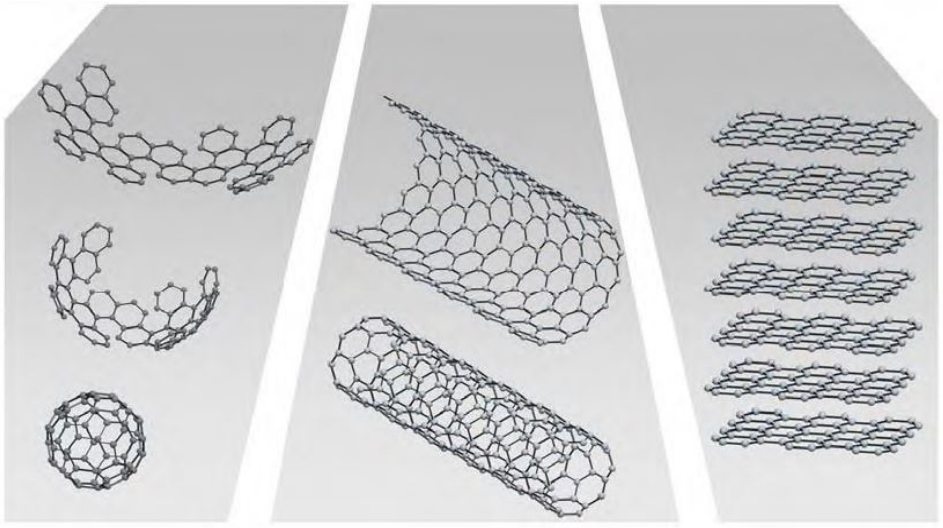

Figure 1.2: Graphene-based molecules: 0D buckyballs, 1D nanotube and 3D graphite.

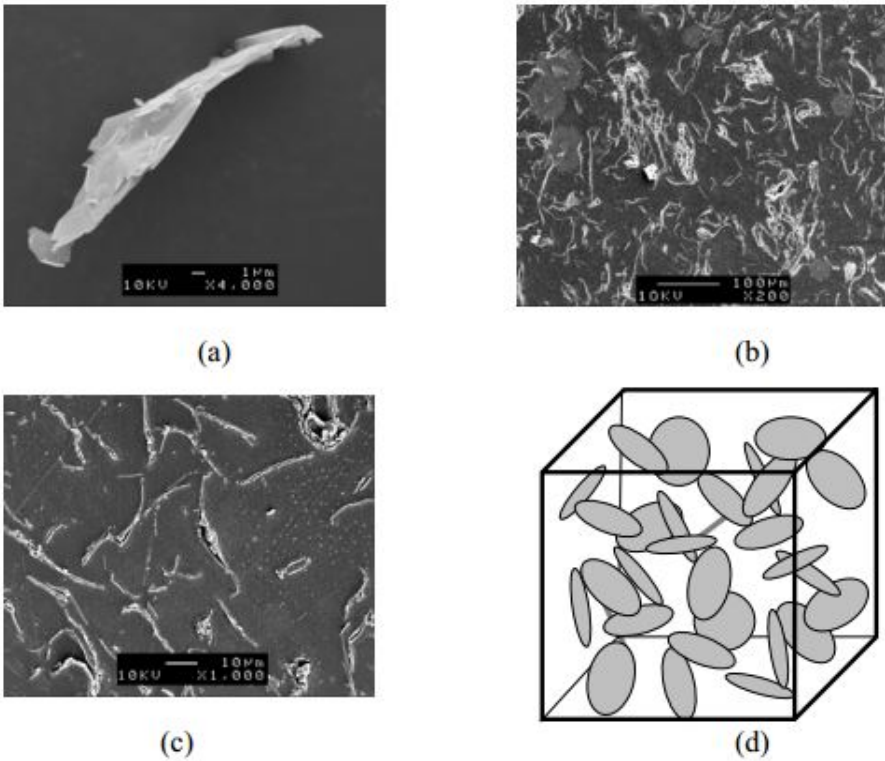

Figure 1.3: Scanning electron microphotographs of (a) GNP particle, (b) and (c) random distribution of GNPs within the epoxy matrix; (c) 3D schematic model of GNP conductive network.

The rapid development of electronic devices has led to some of the most important technologies in materials science, especially for advanced polymer materials. Because electronic devices become smaller and lighter, polymer materials need to have excellent electrical conductivity, thermal stability, significant mechanical strength as well as the ability of maintaining lightness and lost cost. Conventional polymeric materials usually exhibit low modulus and poor electrical conductivity. Combined with other materials the polymeric material can enhance mechanical properties. However, most applications are often limited in the field of electrical engineering because of its electrically nonconductive properties such as fiberglass and ceramic [4]. Since graphene has excellent electrical conductivity and high mechanical strength, composite fibers consisting of graphene take advantage of the high strength and also have the ability to conduct electricity [5], [6]. Material conductivity is significantly improved because graphene has a 2D lattice of sp^2 bond carbon and extremely high aspect ratio. Furthermore, graphene layers are dispersed into polymers that produce multiple conductive pathways in the composites that also improve the conductivities [7]. Combined with high-density polymer, GNP can greatly enhance the mechanical and thermal properties of composites. In summary, graphene possesses a wide range of unusual properties and these properties hold a great promise for industry applications.

1.1.2 Preparation of graphite nanoplatelets and graphene sheets

Many studies have been developed to create single layer graphene. Substantively, preparation methods can be classified into three different routes: (1) mechanical peeling. (2) Epitaxial graphene growth and (3) solution-basted reduction of graphene oxide. By using "Scotch tapes", mechanical peeling method can repeatedly produce graphene sheets of up to 10 μm in planar size [8]. Although this handcraft technique provides crystals of high structural and electronic quality, the graphene sheets produced in this way can only be used for basic research and for making proof-of-concept devices in the predictable future. The alternative route growing graphitic layers epitaxial on top of other crystals [9]. The epitaxial graphene sheets are produced by treatment of silicon carbon (SiC) wafers at high temperature. The epitaxial growing extends to three-dimensions and the epitaxial layers remain bound to the underlying substrate. After cooling down, the graphene layers can be removed from the substrate by chemical etching. Basically, the graphene produced in this technique is impossible to be one-atom-thick crystals. The quality of the graphene highly depends on the substrate materials. Obviously, the above two methods are extremely laborious and inefficient; meanwhile, the quantities of production are extremely small [8] [9]. In order to produce large quantities of graphene, the solution-based route has emerged as a promising approach. In this technique, graphite oxide (GO), which is produced from oxidation of graphite, is used as a medium to obtain stable graphene dispersion in a solvent. GO is strongly hydrophilic and easily exfoliated in water due to its basal or edge plane contains immense amounts of functional groups such as hydroxyl, carboxyl, carbonyl and epoxide. Because the carbon atom is transformed

from a planar sp^2-hybridized geometry to a distorted sp^3-hybridized during graphite oxidation process, GO loses its excellent electrical properties and became an isolator. In order to recover the electrical conductivity, GO must remove most of the functional groups so that the aromatic graphene networks are restored [9]. In large scale operations where engineers utilize large quantities of graphene for industrial application such as energy storage, GO is the most obvious solution due to the relative ease in creating sufficient quantities of graphene to the desired quality levels.

1.2 Simulation Methods

Prior researches in the field of electrical fiber composites were mostly experimental. The manufacturing techniques of composite samples, experimental conditions, polymer matrix, and surface treatment of carbon fibers were the main focuses. While these works provided first-hand information about the various important factors, validations of theories as well as new directions for further research. The limitation of experiments is that composite cannot include every single combination of different factors [10]. Indeed, the complexity can go far beyond the reach of present analytic methods. Due to this reason, many computational simulations as "virtual" experiments appeared. Since the computer simulation can be used to simulate the complex systems, it provides an approach to design the next generation of conductive polymer matrix composites, in which the conduction and percolation behaviors of conductive composites with short fibers embedded in a thermoplastic polymer need to be thoroughly investigated. There are two methods that can used to study the electrical and thermal conductivities,

namely the analytical approach and the Monte Carlo simulation. Both have been extensively used to study percolation phenomena.

1.2.1 Analytical and semi-analytical approaches

The analytical methods can be defined as any computer applications that contain closed form solutions to a system of ordinary or partial differential equations. By using numerical iterations, these equations can be solved and many properties can be estimated including mechanical, thermal and electrical properties. Analytical approaches make it possible to study complex systems by gaining insight into the system behaviors that could be inaccessible using other methods. The closed-form approximate solutions from the analytical methods can bridge the gap between theories and experiments. With these methods some material properties become predictable that would be otherwise difficult to measure from experiments [10], [11]. For the percolation problem, one of the most useful analytical methods is the effective medium theory (EMT). The theory was first developed by Kirkpatrick [29], who investigated the fiber orientation angles and surface contact. He indicated that near the percolation threshold, the behavior should be a general feature of transport in continuous media. He developed a new method called self-consistent effective medium theory (EMT), to deal with more complex transport processes with the Monte Carlo data far away the percolation threshold. This extension of the percolation theory described that except close to threshold, the model based on bond percolation was accurately identified. In addition, the model can also treat continuous media or situations less drastic than the percolation models, for example, materials in which local

conductivity has a continuous distribution of values. Figure 2.1 demonstrates the site percolation probability $P^{(a)}(x)$, for three different 3-D lattices, plotted as a function of the fraction of sites present. Circles represent Monte Carlo data obtained (Kirkpatrick, 1973), crosses indicate face-centered cubic (fcc) and body-centered cubic (bbc) lattices (Dean and Bird 1966). As we can see, the EMT can be used to estimate the effective properties of multiphase materials for a wide range of volume fractions, but these methods are difficult to use to measure the material system containing stochastically distribution with three-dimensional fillers.

Deng and Zheng [59] in 2008 developed an analytical model for the effective electrical conductivity of CNT composites. In the model, the analytical model not only considers the CNT concentration and percolation, but also CNT conductivity anisotropy, aspect ratio, and non-straightness. The supermechanical, electrical and thermal properties of carbon nanotubes (CNTs) have led to increasing interests in studying CNT-based devices and composites. For CNT-in-polymer composites with usual polymer electrical conductivities 10^{-16}-10^{-12} S/m, very low percolation thresholds have been observed. As shown in Figure 1.5, within a narrow range of f near the percolation threshold of critical volume fraction f_{CVF} (typically <1%), the effective conductivity increases dramatically up to about 100,000,000, and the effective conductivity can be improved for 1000 times or much more as f increases up to 10%.

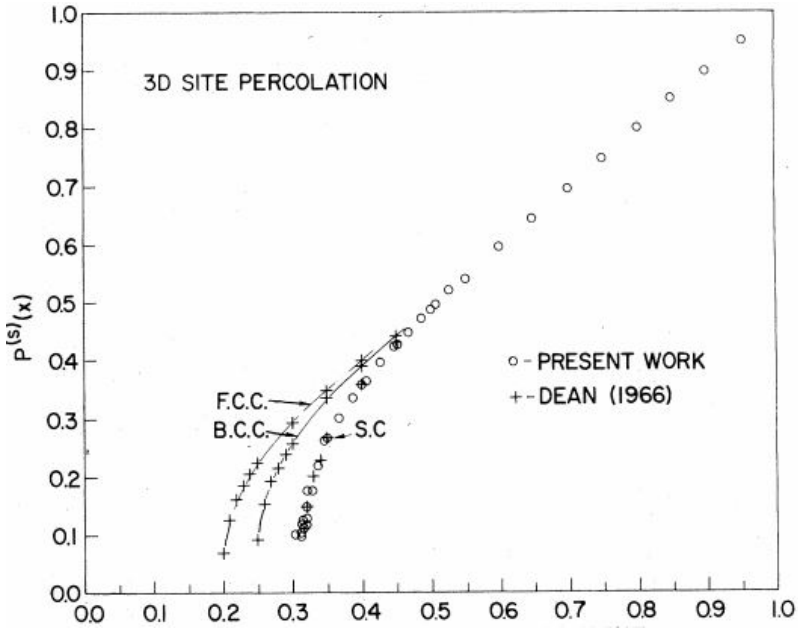

Figure 1.4: X-Fraction of sites present

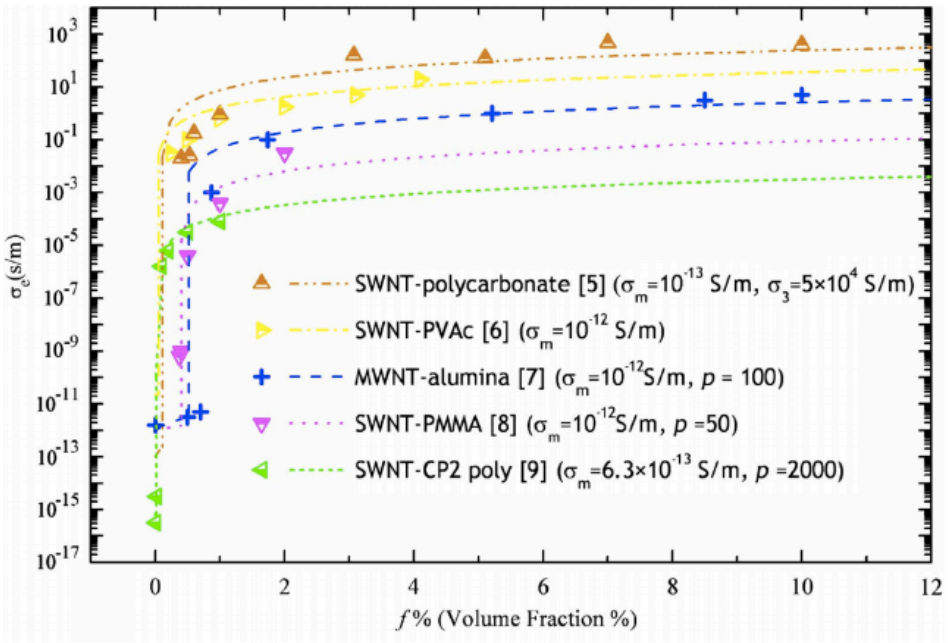

Figure 1.5: Model predictions of the effective electrical conductivities of CNT composites.

Although the analytic method is one of the most vastly used numerical tools, in a number of circumstances this method is computationally prohibitive owing to the small time scales required. While there have been many studies on the physical properties prediction for the composite materials using homogenization methods, in the situation of heterogeneous particulate or fibrous materials, connection between the fibers is determined by the probability of the geometric percolation. In other words, the transport properties of the material system are strongly correlated to the percolation phenomenon. For the heterogeneous material, traditional analytical method cannot predict the properties very well. Instead the Monte Carlo simulation scheme must be used to determine the overall statistical behaviors.

1.2.2 Monte Carlo simulation

Monte Carlo simulation (or Monte Carlo experiments), which contains a broad class of computational algorithms, can explore the sensitivity of a complex system by varying parameters within statistical constraints. The computational algorithms depend on repeated random sampling to obtain numerical results; usually the algorithm runs many times in order to obtain the distribution of an unknown probabilistic system. These systems include mathematical, physical, even finical models. The results from the simulation are analyzed to determine the characteristics of system. An outline of the algorithm is [12]:

(1) Generate a particle at random.

(2) Lump all possible new positions of this particle into sets defined by the new coordinates of the particle and calculate the transition probabilities of movement to each these sets.

(3) Choose one of these sets at random using the computed probabilities.

(4) Choose a position within the chose set at random.

(5) Accept or reject the resulting configuration on the basis of particle overlap.

There are several advantages of Monte Carlo simulation. First of all, the probability distributions within the model can be easily and flexibly used without any approximation. Second, correlations and other relations and dependencies can generally be easily extended and developed as required. In addition, the Monte Carlo method can be easily understood without high level knowledge on mathematics. Furthermore, the changes of the system behavior in response to the variations in the parameters can be investigated. However, the solutions are not exact. The accuracy in the solution depends on the number of repeated runs used to produce the output statistics and usually this method requires an extremely long computational time [13], [14].

1.3 Finite Element Analysis (FEA)

The finite element analysis (FEA) is a useful and powerful computational technique to approach the engineering problems that usually have complex domains by using the approximate solutions with general boundary conditions [15]. FEA is an essential step in modeling of a physical phenomenon or a continuum of matter (solid, liquid, or gas) that contains several field variables. Since the variables vary from point to

point, thus there exist an infinite number of solutions in domain. FEA divides the domain into sub-domains with a finite number of elements or nodes and constructs systematic approximate solutions by applying the variable in variation or weighted residual methods. In other words, FEA simplifies the complex problem into a finite number of unknowns by dividing the domain into elements and by using approximate interpolating functions to express the variables. These functions are defined in terms of the values of the field variables at certain locations, or nodes. Nodes connect adjacent elements and are located along the element boundaries. In summary, FEA is a numerical procedure that can be used to obtain solutions of many engineering problems involving stress analysis, heat transfer, fluid dynamics, composite materials, etc. [16]

The electrical and thermal conductivities of the composite can be predicted by analytical approaches as well as finite element analyses. FEA can be incorporated to investigate the effect of microstructural properties such aspect ratio, interfacial thermal resistance, volume fraction, and filler and fiber dispersion to determine the effective thermal conductivity of a composite. Besides, the filler interactions and chain formation that affect the thermal conductivity of a composite can also be determined by FEA. Fillers have different shapes such as rectangular or circular ones. Therefore, FEA usually requires generation of a new model for every geometry and this process could be numerically intensive [15], [16]. To overcome the model creation difficulties, usually, one can use the commercial FEA software such as Abaqus or ANASYS to generate an input file with the appropriate geometric descriptions. In this work, we use Abaqus to perform the relevant finite element analyses. Abaqus is a general-purpose finite element modeling package for numerically solving a wide variety of problems that include

static/dynamic, structure analysis (both linear and nonlinear), heat transfer, and fluid problems, as well as acoustic and electromagnetic problems. In conclusion, in the finite element solutions of engineering problems, the main procedure includes mesh generation, processing (numerical computations) and graphical representation of results. The user can interact with all three parts in a single environment with embedded functionalities under a same shell (or interface) in separate sections (modules) of a software package. FEA can deal with two-dimensional composites with inclusions of various shapes. The elements can be extended to three dimensions and capture the effect of changes in the volume fraction of the fillers, the filler aspect ratio, the filler dispersion, the interfacial thermal resistance, the filler-filler interaction and the filler orientation effects. Developing the "automated finite element analysis" can explore the effective composite thermal conductivity, and it can be used as an optimization tool in the development of new composites with different constituent materials, microstructures, and filler shapes. Another advantage of the "automated finite element analysis" is that the electrical and thermal conductivities can be determined without analytical models, as one of the shortcomings of the analytical models is its inability to handle fillers with a mix of two different materials or shapes [18].

So far, not much work has been done in the literature related to the effect of microstructural characteristics such as filler interaction and filler aspect ratios in presence of voids and interfacial thermal resistance on the electrical and thermal conductivities of composite. Zhang and Yi [10] conducted a research on the conductivity of short fiber random networks in three-dimensions. In their study, the fibers were treated as cylinders with each cylinder consisting of a nonconductive core covered by a permeable conductive

layer. Monte Carlo simulations was used to evaluate the conductivity and the several factors which include the volume fraction, the solidity of fibers, the thickness of the coating layer, the fiber aspect ratio and the distribution of the fiber orientation angles. By discretizing the interconnected surface of individual fibers, they introduced a finite element method to measure the equivalent electrical conductivity. In the simulation models, each fiber was modeled as a solid cylinder covered by a thin layer of coating material. The nonconductive solid core was not modeled because the nonconductive matrix was not considered. After generation of the solid cylinders, each fiber was discretized into a finite element mesh by using the commercial software MATLAB® and COMSOL® and the generated nodes were subsequently used for a three-dimensional Delaunay tessellation which was used to generate indices of points making up tetrahedrons in the tessellation of the nodes. By using FEA, they determined the relation between the volume of the coating material and the overall effective conductivity. In addition, inserting an insignificant amount of fibers (3%-5%) can enhance the conductivity near the percolation threshold. The effect on the conductivity also significantly increases with the aspect ratio of fiber. Lastly, conductivity is strongly dependent on the fiber orientation angle. When the fibers are aligned with the direction of electric current or the applied potential gradient, the conductivity reaches its maximum.

CHAPTER TWO: CONDUCTIVITIES AND PERCOLATION OF DISK-SHAPED PLATELETS

2.1 Background of Percolation Theory

As mentioned previously, we desire to develop the composite materials that have high electrical and thermal conductivities because these materials have many promising applications such as nanoelectronics, sensors, transistors and batteries. For example, the individual graphene that has excellent electronic transport properties can be used as fillers in advanced composites. In particular, the percolation threshold for graphene-polystyrene composite is ~0.1 Vol% at room temperature, and ~1 Vol% graphene in the composite can lead to a materials electrical conductivity over ~0.1S/m [18]. However, it is very difficult to predict the conductivities of these materials, especially for the short-fiber reinforced composites. Although there are a variety of studies on homogenization method to predict the physical properties for composite materials, it is difficult to apply this method to a three-dimensional fillers material system because it contains inclusions of a random distribution. The transport properties of heterogeneous fibrous materials are strongly connected to the percolation phenomenon in which the material connectivity is determined by the onset probability of the geometric percolation. In the physics and chemistry, percolation is related to the movement and filtering of fluids through porous materials, and it is typically related to conduction problems in heterogeneous materials

[8]. Studying the percolation problems promotes the understanding of many other physical systems. Moreover, the concept of fractals, which is directly related to the percolation theory, is of general interest as it appears more or less everywhere in nature. The knowledge of percolation, fractals and scaling are of tremendous importance in predicting the conductivity of composites. The most common percolation model is a regular lattice system such as square lattice, as shown in Figure 2.1. Let us create a random network by randomly "occupying" sites (vertices) or Bonds (edges) with a statistically independent probability *p*. At random, a site could be occupied with probability *p* or unoccupied with probability 1-*p*. If we define a cluster as a set of occupied sites that can be traversed by jumping form neighbor to occupied neighbor, then site percolation theory is the study of clusters [60]. The site percolation problem has a counterpart called bond percolation: in a lattice, each bond between neighboring lattice sites can be occupied with probability *p* and empty with probability (1-*p*) [61]. Figure 2.1 shows both site and bond percolations, with the left figure being the site percolation that considers the lattice vertices as the relevant entities, and the right figure being the bond percolation that considers the lattice edges as the relevant entities.

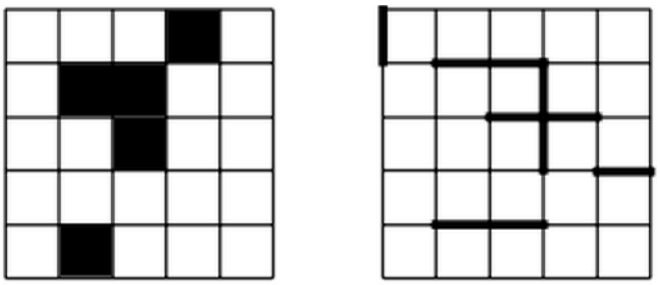

site percolation *bond percolation*

Figure 2.1: Site percolation and bond percolation.

Broadben and Hamersley first studied the theory of percolation in 1957. They studied lattice models for the flow of a fluid through a static random medium, and found that when active medium concentrated is smaller than certain nonzero threshold value, there is no fluid can flow in the system. They also introduced the concept of percolation probability that is sufficiently well connected to the rest to be available for conduction at given region of the medium [29]. In the field of physics, Stauffer in 1985 used computer simulation to study the percolation theory [21]. Balberg determined the fractal dimension of clusters and conductivity of exponent, *t*, on both two- and three-dimensional system. After extensive developments by various researchers, the theory has been a very important branch of statistical physics, and has led to successful applications in a diverse range of problems including hydrology, conceptualization of geometrical and topological characteristics of porous media, and design of electronic and magnetic materials. The percolation theory provides universal laws that have the supreme advantage in determining the geometrical and physical properties of a heterogeneous system [22].

To explain the electrical conductive behavior of composite, we consider the electrical conductivity of composites near the percolation threshold that follows a power-law relationship:

$$\sigma = \sigma_0 (\eta - \eta_0)^n \qquad (2.1)$$

where σ is the electrical conductivity of composite, σ_0 is the electrical conductivity of the filler, η is the probability of site or bond, η_c is the percolation threshold, and n is a conductivity exponent. In the above equation, n is determined by a number of factors

including the particle shape, particle orientation, and polymer-particle interaction, etc. In addition, the value of n is not a constant. However, n and η_c can be determined by curve fitting on the experiment results with different particulate composite systems [23].

2.1.1 Percolation threshold

In order to precisely determine the transition when percolation occurs, we run a number of different simulations where the density of the sites or bonds changes every time. To determine the exact position of the percolation threshold, we can run a series of simulations and extrapolate results with increasing lattice sizes. In other words, the percolation threshold is a characteristic value for a given type of lattice. For different lattices different percolation thresholds are found.

Not only the lattice sites can affect the percolation, but also bonds. Changing the number of neighbors in a given lattice can also affect the percolation threshold. By looking at values for different lattices in Table 1, we can find that different geometries have significantly different thresholds [24], [25].

Table 1 Site and bond percolation thresholds for different lattices

Lattice	Site	Bond
Cubic(body-centered)	0.246	0.1803
Cubic(face-centered)	0.198	0.119
Cubic(simple)	0.3116	0.2488

Diamond	0.43	0.388
Honeycomb	0.6962	0.65271
4-hypercubic	0.197	0.1601
5-hypercubic	0.141	0.1182
6-hypercubic	0.107	0.0942
7-hypercubic	0.089	0.0787
Square	0.592846	0.50000
Triangular	0.50000	0.34729

The lattice geometries with neighbors have lower thresholds while the geometries with fewer neighbors have higher values. For instance, the honeycomb lattice has the highest 2D threshold whereas the triangular lattice has the lowest threshold.

2.1.2 Order of the parameter

Considering now the occupation probability $\eta > \eta_c$, there always exists a spanning cluster. However, how do we determine the number of sites belonging to the biggest cluster? More precisely, can we define the fraction of sites, which belongs to the biggest cluster σ as a function of the occupation probability η? The measure is called the order parameter. Obviously for $\eta < \eta_c$ the order parameter is 0, since there are no spanning

clusters. For $\eta > \eta_c$ the order parameter is increasing. Near the percolation threshold region, the behavior between t and σ follows a power law that is called "universal criticality". This concept of universality of critical phenomena is a framework or theory that describes many different systems [24], [25].

2.1.3 Continuum percolation theory

The continuum percolation theory is a branch of probability theory that extends discrete percolation theory to continuous space. More specifically, the underlying points of continuum percolation are randomly positioned in some continuous space and form a type of point process. For each point, the shapes can be random and the shapes overlap each other to form clumps or components. In continuum percolation, a common research interest focuses on the conditions of occurrence for infinite or enormous components. Other analysis techniques and concepts in this type of percolation theory concentrate on the study of random graphs and random geometric graphs.

Many scientists interest continuum percolation because it shares various mathematical properties with lattice percolation; meanwhile it is a more accurate model for many disordered materials (i.e., porous media, composite materials, polymers, and colloids). Different types of continuum percolation including the distribution of rods, squares and disks and spheres are coming into focus by scientists [25], [26]. Hence, we will introduce several studies of different shape fillers that affect the continuum percolation. For the distribution of rod, one of the obvious examples is a carbon nanotubes-based composite. Carbon nanotubes is entering people's horizons as it has excellent conductivities. Many researches focused on how the nanotube fillers affect the

percolation threshold, which significantly depends on the aspect ratio (semi-major axis-to semi-minor axis) of the filler particles. Balberg and Binenbaum reported a Monte Carlo study of continuum percolation in both 2D and 3D systems of conducting sticks [31]. They extended the pervious study, which only has isotropic sample of randomly oriented equal-length sticks system. The study depends on the percolation threshold on the macroscopic anisotropy of systems with a preferred orientation of the sticks ensemble as well as on the distribution of the stick's lengths. In particular, the systems' orientation can be determined by either random alignments within a given interval or the alignments, which are normally distributed around a given direction. The results showed that the percolation threshold always increases with the macro anisotropic system. The finite sticks ensembles indicated that in the infinite ensemble the percolation threshold is isotropic by extrapolating the results. The contribution of this result is that it presents the anisotropy dependence of the conductivity in random system is depended by both the percolation threshold and the critical exponent [31], [32].

Due to the unique combination of mechanical, electrical and chemical properties, carbon nanotubes as the most potential electrically conductive fillers have been actively studied in recent years. M. Foygel *et al*. [33] found a critical fractional volume (CFV) combined with the percolation threshold for a randomly oriented nanotubes by using Mote Carlo simulations. In the random nanotube system, nanotubes are dispersed stochastically in a low thermo- or electro-conductive medium. In their research, they treated the nanotubes as capped cylinders ("sticks") with high (up to 2000) aspect ratio interpenetrating in the system. Figure 2.2 shows that the nanotube is treated as a capped cylinder. By studying the variation of the CFV and the percolation clusters density, they

indicated that critical exponent of percolation theory (t) can be calculated. For 3D random systems they found that t decreases generally with an increase in the aspect ratio. In addition, the results of electrical and thermal conductivity of the nanotube suspensions and composites by Monte Carlo simulation were compared to the experimental data [33].

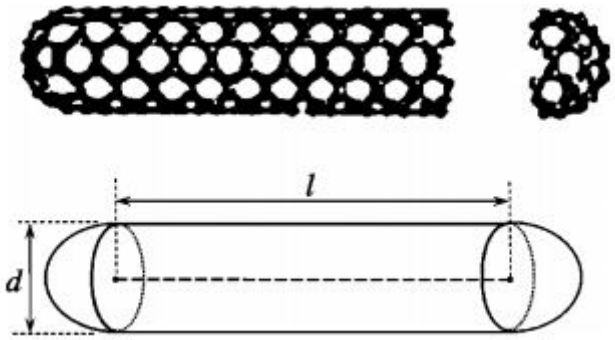

Figure 2.2: Carbon nanotube and its representation as capped cylinder.

Grujicic analyzed the percolation of individual single walled carbon nanotubes (SWCNTs) and of SWCNT bundles dispersed in a non-interacting polymeric matrix by using an analytical model and a numerical simulation method in 2004 [34]. Although prior numerous analytical and numerical models made various successes that include the explanation of the experimentally observed percolation thresholds, it is substantially ignore the potential role that the interactions between fillers can have on the percolation threshold. The interactions, van der Waals force, often significantly affect the random nanotube system and hence must be included into the percolation models. He also developed analytical and numerical models for the percolation threshold and to quantify the effect of such interaction. According to the analytical model, the number of SWCNTs at the percolation threshold, $\tilde{n}_c$, in limit of an infinite nanotube length-to-diameter aspect

ratio, is defined as $\tilde{n}_c = V/Vex$, where V is the specimen volume and Vex is the nanotube excluded volume [34]. The results show that the computed percolation threshold increased due to the van der Waals interactions between the SWCNTs and the associated mutual local alignment of the nanotubes. While the result is comparable to the experimental counterpart, the analytical model is valid only in the case of an infinite length-to-diameter aspect ratio of the dispersed phase. Figure 2.3 shows two different cases: (a) a random distribution of the SWCNTs and (b) the SWCNTs interaction via the van der Waals forces.

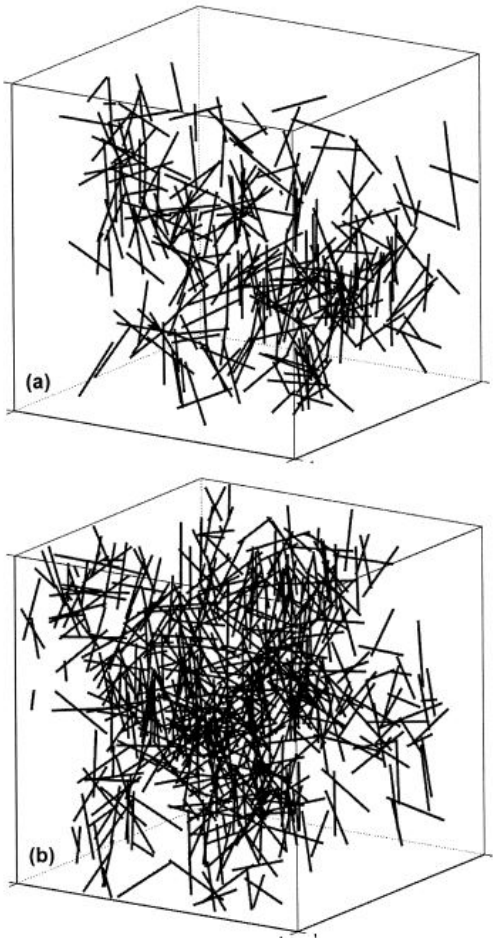

Figure 2.3 Typical structure of a percolating cluster in the cases of: (a) a random distribution of the SWCNTs and (b) the SWCNTs interacting via the van der Waals forces.

In addition to the research on percolation of nanotube and sticks, there are other types of fillers such as spheres, ellipses and disks that have been studied for the continuum percolation properties. Rintoul and Torquato presented a large-scale computer simulation of the continuum percolation model, which consists of a distribution of overlapping (spatially uncorrelated) spheres [57]. The percolation threshold determined from their simulation is η_c=0.2895±0.0005 that is significantly smaller than the value obtained previously using smaller-scale simulations. By using this value they also obtained an estimate of the critical exponent.

Baker *et al*. measured the critical percolation threshold for interpenetrating square objects in two dimensions and cubic objects in three dimensions by using the Monte Carlo simulations [56]. In their studies, two models were presented: (i) particles whose edges are aligned parallel to one another and (ii) randomly oriented objects. For squares and cubes, whose edges are aligned, the critical area fractions at the percolation threshold are η_c=0.6666±0.0004 and 0.2773±0.0002, while for the randomly system, the percolation thresholds are η_c=0.6254±0.0004 and 0.2168±0.0002, respectively. The research confirmed previous results demonstrating the effect of object shape on the threshold for continuum percolation. On the other hand, the research confirmed that randomly oriented particles in continuum percolation significantly affect the percolation threshold. In the randomly oriented squares and cubes system, the particles also have an

average number of bonds per object that is similar to those determined by other researchers for discs and spheres, respectively.

2.1.4 Void percolation

Most of the attention has been given to percolation on regular lattices, even for the study of the particular interest of disordered continuum systems. However, the more appropriate way to explain the continuum percolation such as the structure of liquids or the structure of irregular particle packing is to consider the percolation of the material phase itself. In addition, if the properties of the void space are concerned, the complementary form of percolation is more important. The study of this circumstance is called "void percolation" or "Swiss-cheese percolation" (consider a model consisting of spatially uncorrelated, equal-sized sphere once the spheres are removed from the system) [27]. In overlapping particles system, for example, when the particle density is above than a certain threshold, the particles will constitute large clusters rather than span the whole material system [28]. Although void percolation is not incorporated in our study, many methods related to the studies of void percolation have inspired our research. We will review several studies on void percolation.

Void percolation is very similar to the original definition involving fluid flow through a porous media aforementioned. It is very difficult to predict whether or not there is a connected path for fluid to flow through a system without mathematical tools due to the complexity in the mathematical expressions of the connection functions in void percolation problem. However, this problem can be mapped to the bond percolation

problem on the edges of the Voronoi tessellation (a way of dividing space regions) into a number of the sphere centers.

Since void percolation usually occurs in overlapping circles or spheres with random located centers, we will review some researches on the void percolation first. Kerstein (1983) pointed out that overlapping spheres are equivalent to a bond percolation problem on the edges of the Voronoi tessellation of the sphere centers [35]. He explained the inconvenience of the previous analysis and computations for the void percolation problem due to the absence of an underlying network. Hence, he used a geometrical construction called the Voronoi tessellation to overcome this difficulty. In their problem, they defined the medium to be the union of sphere interiors and the void to be the complement of the medium. The Monte Carlo calculation of the percolation threshold for this problem has provided an estimate of 0.966 for the critical volume fraction [27] [35]. In his article, the result provides a convenient definition of the cluster size and the critical exponents. Elam (1984) *et al.* by using the same model and algorithm simulated the percolation of the void region between overlapping, randomly located spheres [36]. The computed threshold is in a good agreement with the previous result of Kerstein. Meanwhile, three critical exponents were computed and those exponents were found to be in agreement with the universality for a percolation problem with no underlying network. Then, in 1996, Marck developed a network approach to void percolation in a pack of unequal spheres [37]. The procedure was used to calculate the void percolation threshold in a randomly located, overlapping spheres with unequal radii. The threshold from the approach shows universality in both two- and three-dimensions [38]. Although the void percolation and conduction for overlapping spheres are universal by using the

discretization method, those properties with ellipsoidal particles are different. Due to the increased degrees of freedom for the ellipsoidal particles, it is much more difficult to measure the void percolation by using mathematical treatment to deal with the interparticle connectivity. There is no mapping technique to reduce the problem into an equivalent Voronoi tessellation network. Therefore, Yi in 2006 extended a relationship to connect the void percolation and the geometric aspect ratio of ellipsoidal particles [28]. The author used sufficiently small pixels to discretize the system into a fine mesh. With this method, the original continuum system was mapped into a lattice equivalent with a high resolution. The FEM was also used to evaluate the equivalent conductivity of the void phase in the system. The void percolation threshold and equivalent conductivity of ellipsoid was reduced to a traditional lattice problem, and Monte Carlo simulation method was used to identify those properties. The results confirmed that there are no universalities for void percolation threshold and conductivity in particulate system.

Yi also used the computational simulation to measure the void percolation thresholds of oblate particles and thin plate composites by using the lattice mapping technique and the Monte Carlo simulation scheme [39]. Those two types of inclusions are spatially independent and the percolation systems are developed separately based on both site and bond connections. Extrapolation of the results, from those of the finite-size lattices used to the infinite domains, had indicated that the void percolation thresholds of oblate particles have a much stronger dependence on the geometric aspect compared to those of the prolate counterparts. The potential application of his research is that it can be helpful in composite material designs and molecular diffusion problems. In conclusion,

void percolation and conduction associated with elliptical particles of high aspect ratio should be treated differently from spheres.

2.1.5 Percolation threshold for disk-shaped platelets

Since most of our researches focus on the disklike particle composites, we will review the previous studies on the conductivity of the disk plates. From the previous review of analytical models for electrical conductivity of conductive polymer composites we can find that most of the existing models are rods, spheres and close-to-spherical shaped fillers that can only deal with simple geometries. However, for the GNP reinforced polymer nanocomposites, the problem is more complex because fillers in this composite are similar to two-dimensional disks that can distort it or penetrate to each other. Besides, the percolation threshold is much lower than the conventional fillers due to its two dimensional disc-shape fillers that have extremely large surface area and high aspect ratio of GNPs [23]. Compared to the former model, plate-shaped particles can percolate at a much lower volume ratio and therefore have potential applications in engineering practice. Finally, realistic material inclusions can rarely have perfect rods, circular, spherical, or ellipsoidal shapes. Instead, those fillers may have corner angles and facets. How these geometric factors change the percolation properties is still unknown [40].

The disk-shaped filler can be treated as a two-dimensional circular particle with a constant thickness. Regarding the Monte Carlo simulation for disk shape, Seaton and Glandt developed a simulation algorithm combining the generation and acceptance steps

of the conventional method to apply to a two-dimensional system of adhesive disks [12]. The adhesive model is one of the simplest hypotheses, which contain both an attractive and a repulsive part, and it has yielded analytical results to several statistical mechanical approaches. The adhesive model is also an appropriate model for probe of structural inhomogeneous media and particularly system of strongly interacting colloidal particles. Stephan and Cristopher by using the lattice percolation, which consists of microcanonical simulation, efficiently determined the connected clusters, and (in 2D) using exact values from conformal file theory for the probability, at the phase transition, that various kinds of wrapping clusters exist on the torus [41]. The method was applied to percolation in continuum models that contain overlaps between objects with real-valued positions and orientations. By using an algorithm to effectively determine the connected clusters, they found the accurate value of the percolation transition for disks. In the continuum percolations with disks, randomly rotated and aligned as shown in Fig. 2.4, the wrapping cluster is marked by color. In the 2D randomly distributed system, they divided the plane into square bins whose length equals the diameter of the disks. In the given bin, each disk can only overlap or contact with other disks, or in the eight neighboring bins. To simulate the lattice percolation, each time the computer adds a new occupied site and checks which of its neighbors are occupied. If the sites are occupied, the computer will merge them together with the new site. Figure 2.5 shows the methodology to divide the disks in the system. With the help of this approach, they predicted the conformal field theory both for the finite-size scaling exponent n and the probabilities that various kind of wrapping clusters exist at η_c on periodic boundary conditions.

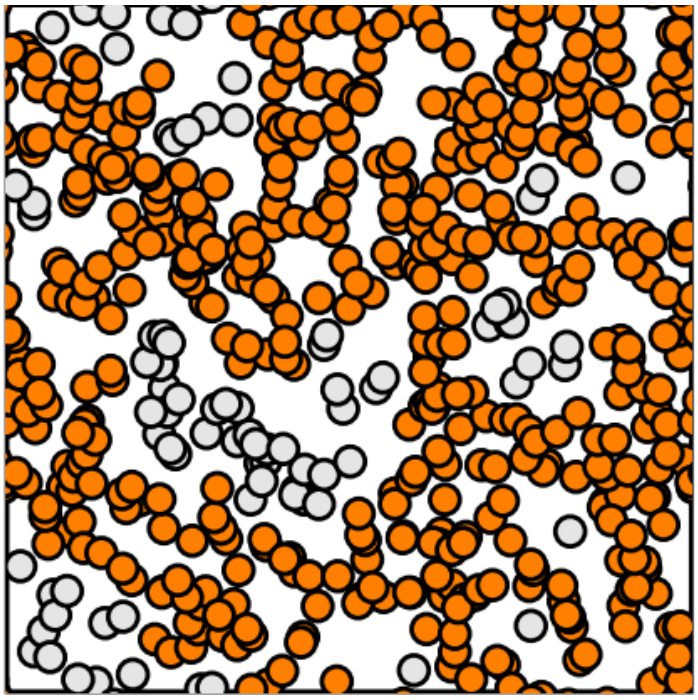

Figure 2.4: Continuum percolation with disks in 2D random system.

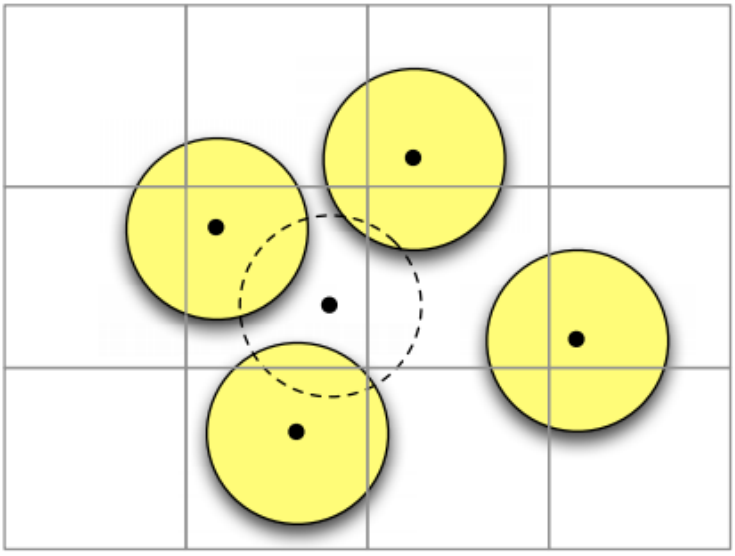

Figure 2.5: Model of adhesive overlapping disks.

Li and Kim (2007) used the average interparticle distance (IPD) concept to predict the percolation threshold of conducting polymer composites containing disc-shaped

nanoparticles with high aspect ratio [23]. Figure 2.6 shows two types of conditions, two- and three-dimensional random orientations, were considered in the model of particle distribution. In this model, particles are homogeneously distributed within the matrix and those fillers are treated as equal size disc-shape particles that bonded with the polymer. It was assumed that the composite is divided into cubic elements each containing one particle in the center, and that the total number of cubic elements is equal to the total number of particle.

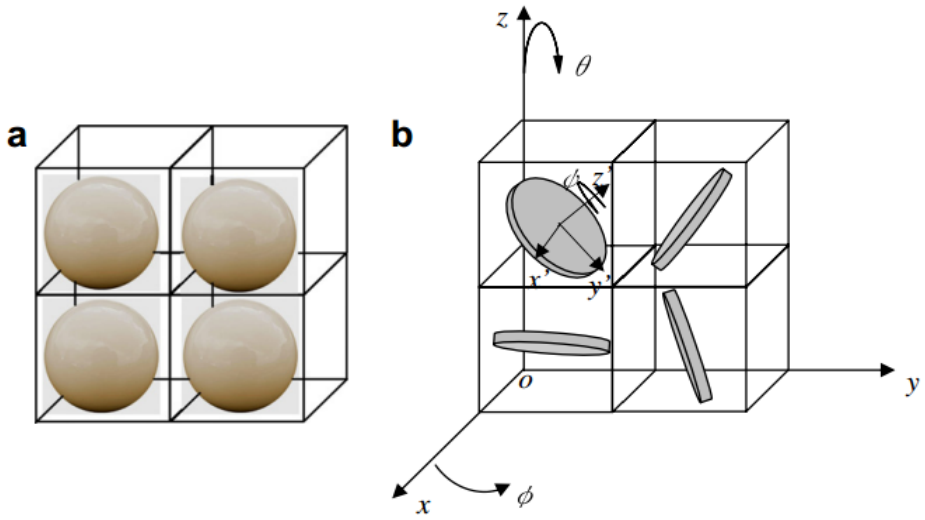

Figure 2.6: Schematic drawing of the IPD model for (a) sphere filler and (b) 3D distribution of fillers with high aspect ratio.

The results show that aspect ratio of conducting filler significant effect the nanocomposite percolation threshold. Compared with the experimental percolation threshold of GNP nanocomposites containing various polymer matrices and theoretical predictions based on the existing models, the present IPD model agreed better with the published experimental data. The parametric study of the IPD model gave insights into

how to minimize the percolation threshold of nanocomposite electrical conductivity by controlling the geometry of conducting fillers.

For the percolation threshold of fully penetrable discs system, Quintanilla and Torquato in 2001 studied the percolation of the system [42]. In the model, an inhomogeneous distribution of fully penetrable discs consisted of a two-phase system and the critical volume fraction was obtained from some specified density gradients. Some particles will connect to the region of high volume fraction, forming a percolation cluster. The authors measured the fractal behavior of the frontier, or the edge of this percolation cluster. They also studied the percolation threshold for a system of statistically homogeneous discs. The values of percolation is η_0=0.676339 ± 0.000004.

Yi indicated a limiting case of oblate ellipsoids that is the ellipsoids' thickness approaches zeros [40]. It is of particular interest because the ellipsoids will be reduced to 2D plates in the 3D space under this circumstance. Four platelike fundamental shapes were introduced: circles, ellipses, triangles, and squares. In his research, a standard computational algorithm for percolation checking has been implemented. All the particles were generated in a unit-cell domain. An appropriate criterion was used to check the connection between the particle as well as the boundary connectivity. The process depended on the intrinsically probabilistic in a finite system and percolation was determined as simply the ratio of the percolation to the total number of simulations performed. Percolation threshold is 50% of the plate number corresponding to a percolation probability. Since the probabilistic variation in the results depends on the plate size or the total plate number, an algorithm was developed to make the process more efficient. The number of implementation depended on the plate size variably. For

larger size plates, the number was set to a few hundred. For small size plates, it was set to between five and ten. This treatment can extremely reduce the variation in the results, thereby increase the accuracy of the solution. Since the plates are oriented in 3D, the statistical invariant obey the cubic function of the characteristic length, the definition of percolation threshold is consistent with that of equivalent 3D systems instead of 2D system. The author defined the following equation to measure the percolation threshold:

$$\eta_0 = \frac{4}{3}\pi r^3 N \tag{2.1}$$

where r is the radius and n is the total plate number. For triangles and squares, r is the equivalent radius of the circular plate having the same area. When r approach to zero, n will become infinite for percolation, but value of η will approach an invariant η_c which is defined as the "percolation threshold" of the system. By extrapolating the data to zero radius, the percolation threshold normalized as follow: η_c=0.9614, 0.8647 and 0.7295 for circles, squares, and equilateral triangles, respectively. The results indicated that noncircular shapes and corner angles in plate enhance the connectivity of interparticle in the system, therefor reduced the percolation point. For elliptical plates, the percolation threshold is found to decrease vicissitudinous, specifically, the aspect ratio ε reduce moderately between 1 and 1.5 and decrease rapidly for ε greater than 1.5. For the binary dispersion of circular plates with two different radii, η_c consistently larger than that of equalized plates, with the maximum value located at around r/r_1=0.5.

We have already reviewed several studies on disklike particles for the overall electrical conductivity of composite by using the finite element method [43], [44], [45].

Some other researchers in this area include Robers and Garboczi who studied material properties of random porous composite with various microstructures [45]. However, reduction in local maximum errors, particularly at material boundaries, is not guaranteed in that method. In an alternative approach Cai applied this concept to compute thermal conductivity of PTEE composite [45]. In general, the finite element modeling of multiphase heterogeneous composites is by no means a routine task, since the fibrous or particulate inclusions are interconnected. The persistent obstacles to mesh automation of complex structure are well known and no individual commercial solver is capable of handling these difficulties. Development of a new, direct simulation method that does not rely on digitization of the material phase, thus allowing more accurate modeling of the interconnected structures, is therefore of great importance.

2.1.5 Binary mixture of disks

Measurement of the percolation threshold for spheres, ellipsoids, and disks has received much attention in the literature and achieved a lot of successes. However, little research had been performed for the percolation problems for systems of disks with different radii. Mohan and Dhar (1984) studied the related geometrical problem of random percolation of overlapping discs with a distribution of different radii [46]. In the article, the author considered continuum disc percolation in two dimensions. The positions of the discs are consistently distributed on a 2D plane, $n(R)\,dR\,dA$ being the probability that the center of the disc having radius between R and $R+dR$ lies inside a small area dA. The total area of discs per unit area of the plane is:

$$\rho = \int \pi R^2 n(R) dR \tag{2.2}$$

ρ will be called the areal density of the discs. The average fractional area of the plane that contains at least one disc is easily shown by the formula 1-exp (-ρ). When the radii are equal, the percolation threshold is independent of the size of the disks. The result of this article shows that the percolation threshold of different radii of disks is different from that of monodispersed disks. The overlapping discs having a distribution of radii, the net areal density of discs at percolation threshold depends on the distribution of radii and is not bounded by any finite constant [39]. However, this study made no attempt to study the nature of the threshold's dependence on the implicit distribution of radii.

Quintanilla (2001) measured the percolation threshold for two different systems of fully penetrable disks with variable radii by using the gradient percolation [46] [47]. To estimates the previous percolation thresholds, the authors added two decimal places in the results in both systems. In this research, the results also show that if the radii follow a uniform distribution, the percolation threshold is 0.686610. For the binary dispersions, the influence of constitutive parameters on the percolation threshold was also studied. With the appropriate parameters, the percolation threshold of penetrable disks of different radii approximately achieved 0.76. Although using gradient percolation for soft disks of two different radii were performed in 2D in their research, the method cannot be applied in three dimensions.

Consiglio *et al.* (2003) measured the percolation threshold of a mixture of spheres A and B of two different sizes, *v*A and *v*B in 3D. [48] They show that the continuum percolation threshold is dependent on the relative concentration of the two different sized

spheres. The method used in this article is based on the Leath algorithm and the Lorenz and Ziff method, which use Fisher's scaling function. By using Monte-Carlo simulation, the result for the continuum percolation threshold of a three-dimensional mixture of spheres of two different sizes was obtained. They fixed the value of r to obtain the threshold for various values of x, the ratio of the number of larger objects to the number of total objects. The critical volume fraction increases from η_c=0.28955 for equal-sized spheres to a maximum of η_c=0.29731.

It should be pointed out that despite the successful work on the percolation problems, a systematic study of the conductivity of randomly oriented disks is not widely available in the literature. In this study, an efficient computational algorithm for determining conductivities will be implemented. We will first establish an element partition scheme as well as a set of criteria for detecting interparticle connections followed by a finite element analysis. Then the curve fitting techniques will be applied to estimate the percolation threshold along with the key parameters in the power-law approximations.

2.2 Simulation Method for Disk-shaped Platelets

In this study we assume a system of circular disks with negligible thickness uniformly distributed in a three-dimensional unit cell. Hence the centers of the disks are distributed with a constant probability density function, as shown in Fig. 2.1 The disks are fully penetrable and the orientation angles of the axis (i.e. the normal of disk planes) are also randomly distributed, following a particular probability density function [49].

These disks form clusters and therefore the first necessary step in our modeling is to detect the pairwise connectivity of the disks.

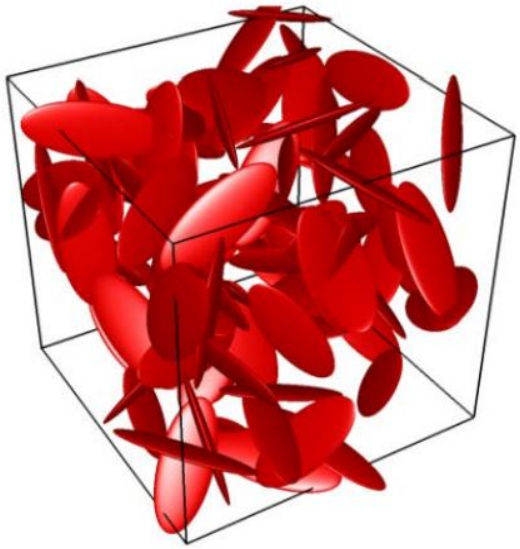

Figure 2.7: A computational model showing a system of random circular disks.

2.2.1 Intersection criteria

Given two circular disks of radii r_1 and r_2, by modifying the previously reported technique [7] we developed the following intersection criteria in a more efficient way. We first determined the normal vectors $\vec{n}_1$ and $\vec{n}_2$ of the two disks based on their orientation angles. Assuming $\vec{R}$ to be the position vector from the center of the first disk to that of the second, we defined the following quantities:

$$\beta = \frac{\vec{R} \cdot \vec{n}_1}{\sqrt{1-(\vec{n}_1 \cdot \vec{n}_2)^2}}; \tag{2.3}$$

$$a,b = \pm\sqrt{R_2^2 - \beta^2} + \frac{\vec{R}\cdot(\vec{n}_1 \times \vec{n}_2)}{\left\|\vec{n}_1 \times \vec{n}_2\right\|}; \tag{2.4}$$

$$c = \frac{\vec{R}\cdot(\vec{n}_1 \times (\vec{n}_1 \times \vec{n}_2))}{\left\|\vec{n}_1 \times (\vec{n}_1 \times \vec{n}_2)\right\|} - \beta(\vec{n}_1 \cdot \vec{n}_2); \tag{2.5}$$

$$p = \sqrt{r_1^2 - c^2}; \tag{2.6}$$

It can be proved that the two disks intersect if and only if $r_2^2 - \beta^2 > 0$ and any of the following four conditions is satisfied:

$$\text{(i) } a^2 + y^2 \le r_1^2; \tag{2.7}$$

$$\text{(ii) } b^2 + c^2 \le r_1^2; \tag{2.8}$$

$$\text{(iii) } \left\|c\right\| < r_1 \ \&\ (a-p)(b-p) < 0. \tag{2.9}$$

$$\text{(iv) } \left\|c\right\| < r_1 \ \&\ (a+p)(b+p) < 0. \tag{2.10}$$

The above criteria have been validated by a computational realization of the random disks in Matlab, followed by an inspection of the actual interparticle connectivity. In the next step we discretized the interconnected system to construct a continuous mesh for the subsequent finite element analyses.

2.2.2 Element generation and partition

The finite element analysis is the key step in the entire procedure to determine the equivalent conductivity of the disk system. In general, mesh generation is not a

technically challenging problem, since numerous commercial finite element solvers are available in the market and these codes usually contain built-in automatic meshing algorithms. Their common strategy involves the description of the overall surface geometry. For example, a Boolean operation can be applied to a two-dimensional system of overlapping disks to obtain a union geometry. A finite element mesh can then be generated on the resulting geometry. A large, randomized heterogeneous system in three dimensions, however, requires meshing of an immense number of particles in order to minimize the size effects in the subsequent analyses. For volume fractions exceeding the percolation threshold, it is generally difficult to describe the overall surface or volumetric geometries, without resorting to manual techniques.

In this study, we developed a new, automated mesh generation scheme. First, a triangular shell mesh was created on the surface of each individual disk using the mesh generation functionality embedded in COMSOL© [51]. Figure 2.8 shows the disk plate which is divided by COMSOL© into triangular elements. The local mesh density is curvature dependent; therefore a few parameters including the curvature cutoff threshold and maximum element size were defined to avoid excessive local elements and numerical inaccuracy induced by the local singularities of the solution. The elements were then translated and rotated to the locations specified. These triangular elements were later used as a basis to create interfacial elements. The disk size was fixed throughout and varying the disk number made the changing of disk density. The thickness of disk was assumed to be much smaller than the diameter, and therefore no discretization was performed along the thickness direction.

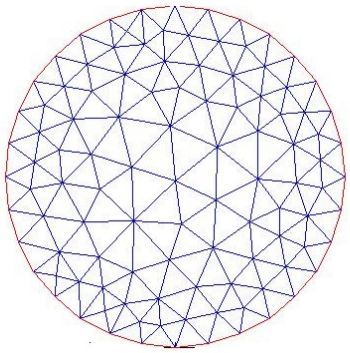

Figure 2.8 Automated mesh generation scheme for the disk filler with r=0.1.

When two disks meet, the two planes form a line of intersection. A standard finite element analysis requires continuous connections of elements at the boundaries. To connect the elements located on the two different planes, a partition scheme was implemented to cut the triangular elements across the line of intersection. A strategy was introduced in the scheme in which we first determined the spatial locations of the intersection points formed by the edges of one triangle and the plane formed by the other triangle, as shown in Fig. 2.2 The line of intersection between the two planes was then obtained by connecting the two intersection points. In Fig. 2.9, the location of the intersection point F of a line DE and the plane defined by the triangle ABC was determined from the following vector operations,

$$\overrightarrow{FD} = \overrightarrow{DE}\left(\frac{|DG|}{|DH|}\right) = \overrightarrow{DE}\left(\frac{\overrightarrow{AD}\cdot\vec{n}}{\overrightarrow{ED}\cdot\vec{n}}\right), \tag{2.11}$$

where

$$\vec{n} = \frac{\overrightarrow{AB} \times \overrightarrow{AC}}{\left|\overrightarrow{AB} \times \overrightarrow{AC}\right|}, \tag{2.12}$$

and

$$\overrightarrow{r_F} = \overrightarrow{r_D} - \overrightarrow{FD} = \overrightarrow{r_D} - \overrightarrow{DE}\left(\frac{\overrightarrow{AD} \cdot \vec{n}}{\overrightarrow{ED} \cdot \vec{n}}\right). \tag{2.13}$$

This method allows for determination of the two intersection points, whose positions relative to the triangle could be categorized into the following cases:

(i) located at a vertex of the triangle;

(ii) located along an edge of the triangle;

(iii) located in the interior of the triangle;

(iv) located in the exterior of the triangle.

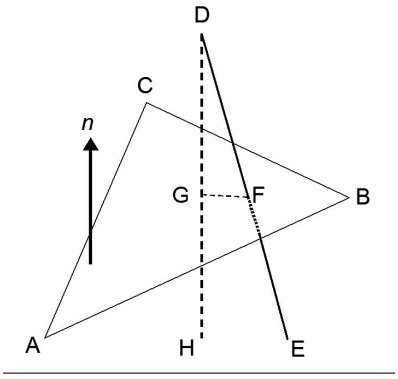

Figure 2.9: A schematic showing the determination of the location of intersection point between a line and a plane constituted by a triangle.

Depending on the locations of the intersection points, an element can be partitioned into multiple smaller elements. From a close inspection of all possible scenarios, we have

found that there exist only five distinct configurations that should be treated separately, as illustrated in Fig.2.10. It turns out that the minimum number of the new elements is two when one of the intersection points is located at a vertex and the other is located on an edge (i.e. case#4); whereas the maximum number of the new elements is five when both points are located in the interior of the triangle (i.e. case#3).

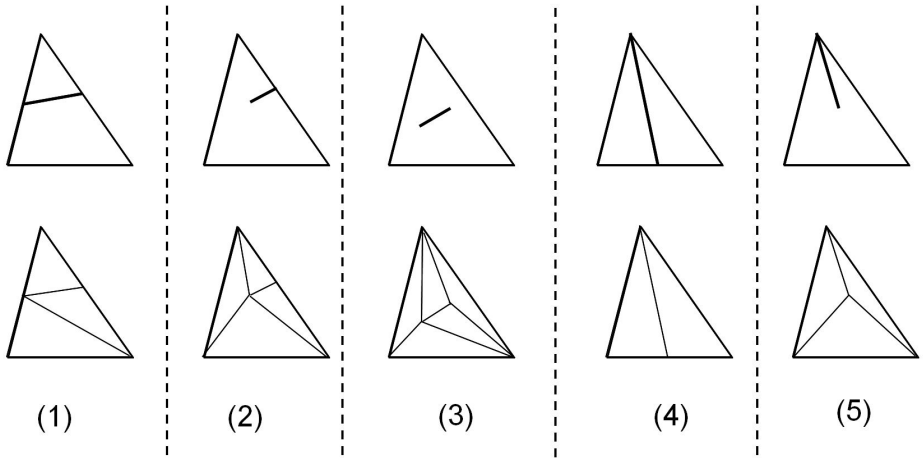

Figure 2.10: Five possible configurations involved in the element partition schemes, with the top row representing the different locations of the line of intersection and the bottom row representing the new elements created by the scheme.

Figure 2.11 shows an example in which two adjacent triangles have been partitioned by a line of intersection. The elements shown on the left and the right represent the configurations before and after the partition was applied, respectively. Multiple results are possible in each case. For example, the triangle on the left in Fig. 2.11(a) can actually be divided into four or more new triangles, rather than three as shown in Fig.2.11 (b) Overall, our objective is to minimize the number of the newly created nodes and elements. In some cases, it is necessary to locate the intersection of

two line segments on a same plane. Suppose AB and CD are two arbitrary line segments located on the same plane. The location of an arbitrary point r (x, y, z) on either of the two lines can be expressed as

$$\begin{aligned} r &= r_A + (r_B - r_A)t \\ r &= r_C + (r_D - r_C)s \end{aligned} \tag{2.14}$$

where both t and s are the local coordinates ranging between 0 and 1. By solving the simultaneous equations for x and y, we have

$$\begin{aligned} s &= \frac{(x_A - x_C)(y_B - y_A) - (y_A - y_C)(x_B - x_A)}{(x_A - x_B)(y_D - y_C) - (y_A - y_B)(x_D - x_C)} \\ t &= \frac{(x_A - x_C)(y_D - y_C) - (y_A - y_C)(x_D - x_C)}{(x_A - x_B)(y_D - y_C) - (y_A - y_B)(x_D - x_C)} \end{aligned}. \tag{2.15}$$

When the two lines intersect, there must be a unique solution to the above equations. To ensure the existence of such a solution, the denominator must be nonzero, leading to

$$\Delta = \left|(x_A - x_B)(y_D - y_C) - (y_A - y_B)(x_D - x_C)\right| > 0. \tag{2.16}$$

Figure 2.12 shows a couple of examples of the element mesh formed by three intersecting disks after the partitions scheme was applied. It can be seen that the continuity is satisfied at the interfaces of the disk planes. For a realistic system containing a large number of disks, the pairwise connections among the disks were examined and the element partition scheme was applied whenever such a connection was detected. A complete finite element model containing 1,000 disks of radius 0.07 and approximately 100,000 elements is shown in Fig. 2.13, using this automated mesh generation scheme.

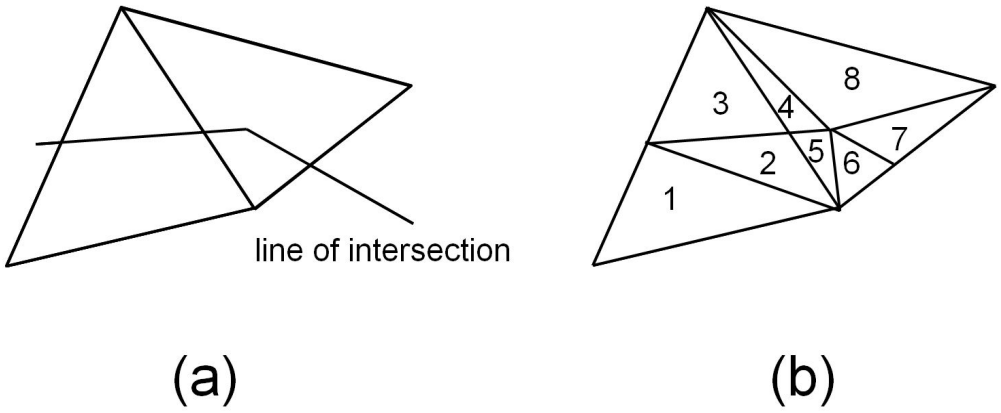

Figure 2.11: An example showing two adjacent triangular elements: (a) before partition; (b) after partition.

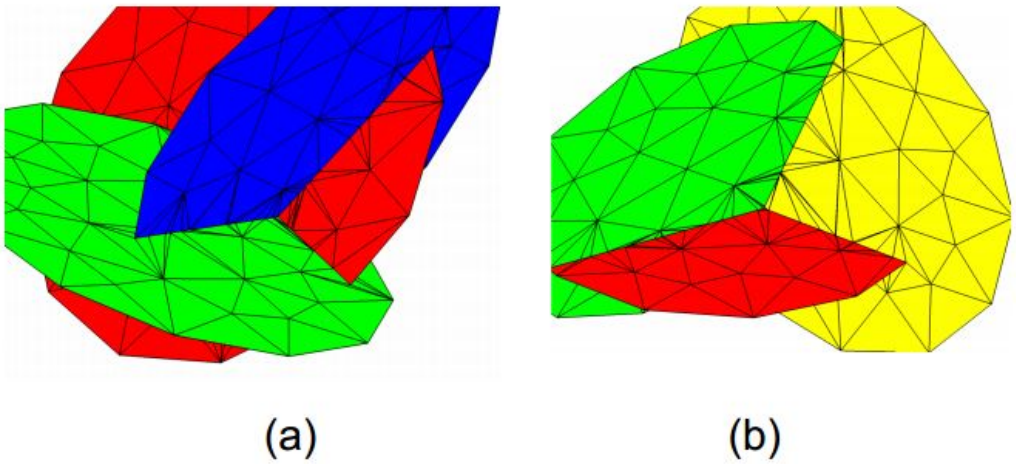

Figure 2.12 Examples showing the finite elements created for a cluster of three disks with the successful implementation of the element partition scheme.

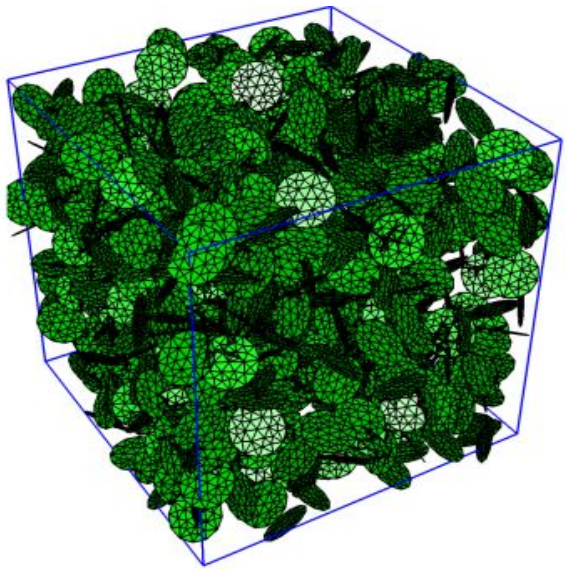

Figure 2.13: A complete finite element mesh for the entire model with 1000 disks of radius 0.07 and approximately 100,000 elements.

2.2.3 Finite element analysis

The mesh data including the nodal positions and element compositions were exported to an ABAQUS® script file. The effective conductivity of the material system was computed from a steady state heat conduction analysis. More specifically, a DS3 element type (namely, three-node triangular shell element for thermal analysis) was selected. The kinetic degrees of freedom were absent and the temperature was the only remaining degree of freedom in the analysis. A unit temperature difference was specified on the two opposite sides of the unit cell and the reactive heat flux was computed. Thermal conduction took place due to the temperature gradient and the steady state solution was sought by solving Laplace's equation. It can be proved that the total flow rate by summing the nodal heat flux is equivalent to the effective conductivity of the

system. Despite the physical distinction between thermal and electrical conductions, the normalized computational result here can be interpreted as either the thermal conductivity or the electrical conductivity because of the mathematical and physical analogies between the two phenomena.

We varied the disk radius from 0.05 to 0.15 in our simulations. The smallest disk size corresponds to one tenth of the unit cell and the largest size is approximately one third of the unit cell. In the former case the boundary effect is negligible whereas in the latter case the boundary imposes a significant constraint to the system. Therefore we were able to study the scaling effect on the simulation results. The simulations were run for 10~20 times at each volume fraction (or equivalently, each number of disks) depending on the disk radius. The results were collected and the means and the standard deviations were computed afterwards.

2.2.4 Percolation threshold of the disk-shaped particles

Theoretically percolation occurs at the transition of conductivity from zero to a nonzero value for an infinite system. In the simulations, the exact location of this transition is highly probabilistic due to the finite size effect and the percolation threshold can be estimated from a statistical analysis of the results. The percolation threshold can generally be expressed in terms of either the area fraction for two-dimensional particles or the volume fraction for three-dimensional particles. In the present study the disklike geometries are two-dimensional but they are oriented in space. We hypothesize that the statistical invariant for disks in three dimensions follows a cubic function of the characteristic length and that the definition of percolation threshold is consistent with its

spherical counterpart. We define the following quantity to measure the percolation threshold:

$$\eta = \frac{4}{3} N\pi r^3 \tag{2.17}$$

where r is the disk radius and N is the total disk number. As r approaches zero, N would become infinite for percolation, meanwhile η would become an invariant η_c. Therefore η can be interpreted as the normalized disk size and will be used throughout our discussion in the remaining sections. We will later verify this hypothesis through simulations.

The application of a mathematical formula to approximate the behavior of a physical system is frequently encountered in the engineering practice. One of the most common techniques is linear curve fitting. This is usually done using a method called "the least squares curve fitting". When a complex equation contains adjustable parameters, it is important to have an error analysis on the constants and information about the mutual dependence of the constants. However, a "good-fit" to the data does not mean that the parameters are individual well determined. Complex problems are frequently "linearized" by selecting experimental conditions that yield a series of straight lines whose slopes and intercepts are fitted by another straight line.

2.4 Curve-fitting method

A general curve-fitting program can provide a test of the goodness of fit of an equation without imposing special constraints upon the data collection. In addition, it can provide for the proper weighing of the individual data points, a procedure weighing of the

individual data points, and a procedure that is often not followed, even for the simple equations. Finally, the use of numerical integration procedures can provide a fit to the data of differential equations.

MATLAB can perform different types of curve fitting based on the simulation results. The two axes in the figure represent the conductivity and the corresponding fiber number. Based on the trend of the data points, we have found that the relationship between the conductivity and the fiber number is non-linear. Meanwhile, the conductivity increases with the fiber number. The data analysis shows that the simulation results fit the power-law function very well. According to the definition of the percolation threshold mentioned in the previous section, for an infinitely large system the transition will occur at η_c. For our simulation data, generally, the equation can also be written as:

$$K = A(N - N_0)^t, \text{ for } N>N_0 \tag{2.18}$$

where K represents the conductivity of the system; N is the fiber number; N_0 is the fiber number at the percolation threshold; and A is the coefficient, which is related to the conductivity of the filler, σ.

First of all, we need to determine N_0 and t, and then use the relation between N_0 and η_c to estimate the percolation threshold. From the data analysis and the percolation theory, we conclude that when $N<N_0$ there are no spanning clusters. In other words, the conductivity of the system is zero. When $N>N_0$, the conductivity and fillers follow the power-law function. To specifically determine each parameter, we have developed a MATLAB function that can solve nonlinear curve fitting problems. In this function, we

use *lsqcurvefit* algorithm that can solve nonlinear curve fitting problems in the least-square sense. That is, given the input data *N*, and the output K, we can find the coefficient N_0 that can "best-fit" the equation:

$$\min_{N_0} \frac{1}{2}\left\|F(N_0,N)-K\right\|_2^2 = \frac{1}{2}\sum_i (F(N_0,N)-K)^2 \tag{2.19}$$

where *N* and *K* are vectors, and $F(N_0, N)$ represents the power law equation. We named the function [*A* N_0 *t*]=*lsqcurvefit* (*K*, *N*), where the input arguments *N* and *K* are vectors with the coordinates of the data points. In order to reduce the computing time and improve the accuracy of the solutions, it is necessary to make an initial guess at the solutions by specifying their upper and lower bounds. The conductivity becomes zero when the filler number *N* is below the percolation threshold N_0. By using the approximation techniques, we can determine the lower bounds of N_0. In this research, the lower bounds of N_0 are 1800, 600, 230, 70, when *r*=0.05, 0.07, 0.1, and 0.15, respectively. For the upper bounds of N_0, once $N > N_0$, spanning clusters will appear in the system. In other words, the conductivity, *K* cannot be all zero in one set of simulation trials. In this work, the upper bounds of N_0 are 1900, 650, 320, 130, when *r*=0.05, 0.07,0.1, and 0.15, respectively. We have determined the percolation threshold of the fiber numbers N_0, however, the exponent value *t* is still unknown. Let us consider the case when $N>N_0$, the system will always exists a spanning cluster. Obviously, when $N<N_0$, *K* is 0 since there are no spanning clusters. As a result *t* must be positive. When $N>N_0$ the order parameter increases. From the curve fitting analysis we find that the relation between the conductivity *K* and the fiber number *N* follows a convex function with the lowest point

close to the percolation threshold. Due to this reason, the lower bound of the conductivity exponent t cannot be smaller than 1. However, there is no such restriction on the upper bound, because the curvature is still unknown. In this work, the upper bound of conductivity exponent is assumed to be 3. For the coefficient A, on the other hand, it is difficult to find its upper bound. From the literature, we have found that the typical value of A ranges between 10^{-5} and 10^{-10}. Once the relationship between the conductivity K and the fiber number N is established, all of the relevant parameters can be easily determined. The percolation threshold can be determined by Eq. 2.20 and the filler conductivity σ_0 can be computed by operating Eq. 2.18:

$$\eta_0 = \frac{4}{3}\pi r^3 N_0, \tag{2.20}$$

and

$$\sigma_0 = \frac{3A}{(4\pi r^2)^t}. \tag{2.21}$$

2.5 Simulation Results for the Disk-Shaped Platelets

There are a few parameters that can affect the conductive performance of material: (1) the diameter of disks; (2) the total number of disks; (3) the disk thickness; (4) the conductivity of the disk material; (5) the distributions of the parameters (including size, center location and orientation angles); (6) the aspect ratio of elliptical plates (semi-major axis-to-semi-minor axis). To simplify the problem we assume uniform distributions of the locations and orientation angles and therefore the last factor is not taken into consideration here in our study.

2.5.1 Effect of disk thickness

We first investigated the effect of disk thickness on the conductivity using a pair of fixed parameters r=0.07 and N=1000. We varied the disk thickness from 0.001 to 0.01 by modifying the solid section definitions of the sell elements in the finite element analysis. From the elemental theory of electrical or heat conduction, a greater size of the cross section allows for a higher rate of conduction. Therefore the conductivity must be proportional to the cross sectional area, and hence the thickness. This has been confirmed in Fig. 2.14, which shows the conductivity as a strictly linear function of the disk thickness. Due to this reason, in the following discussion we define a dimensionless conductivity K that is normalized against the disk thickness, which is defined as

$$K = \frac{K_{eqv}}{K_{disk} h} \tag{2.22}$$

where K_{eqv} represents the computed conductivity of the entire system, K_{disk} is the conductivity of the disk material, and h represents the disk thickness. Because K_{eqv} and K_{disk} have the same unit and h represents the normalized disk thickness, the result of the equation K should be a nondimensional value. Do in this way, the results of the conductivity K can be used to predict the properties of the material in the practical by just multiplying the coefficient of the thickness and conductivity of the particles. In this way we believe that the simulation results can be presented clearly and succinctly.

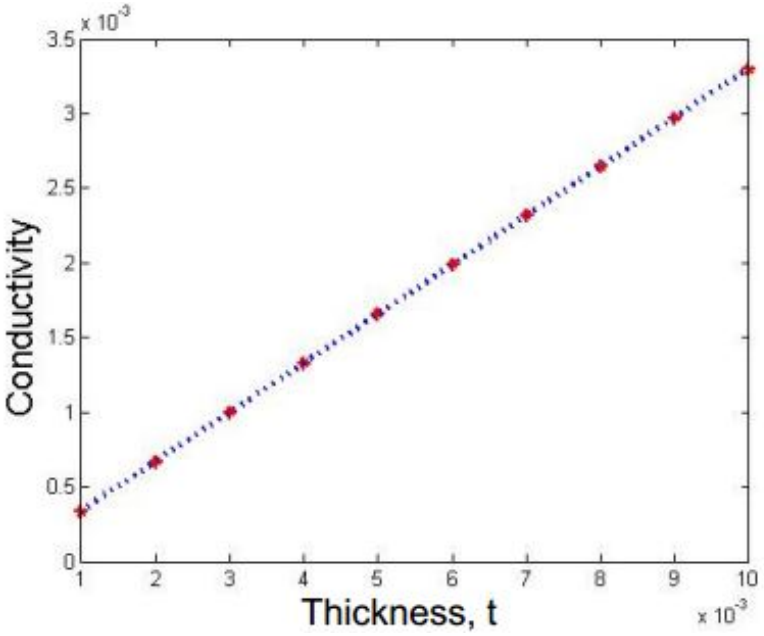

Figure 2.14: Conductivity as function of disk thickness.

2.5.2 Power-law fitting of conductivity

Shown in Fig 2.15 is the simulation results of the equivalent conductivity expressed as a function of the disk number for four different radii ranging from 0.05 to 0.15. The total number of disks varies from 1800 to 70 accordingly. To evaluate the statistical variations, the simulations were repeated 10 or 20 times for each radius, with larger radii requiring more simulation trials. Apparently the conductivity remains zero when insufficient number of disks is incorporated to form conductive pathways in the system. The result becomes nonzero as the disk number reaches a critical value that is equivalent to the percolation threshold. Beyond this critical value the conductivity increases nonlinearly. This is consistent with the results reported in the literature for

heterogeneous materials containing inclusions of other geometrical shapes. In addition it is shown in the figure that fewer disks are present in the model when the disk size increases, resulting in a greater variation. The simulation results can approximately be fitted into a power-law form using the least-squares scheme:

$$K = A(N - N_0)^t, \text{ for } N>N_0 \tag{2.23}$$

Matlab function *lsqcurvefit* has been used in curve fitting and the estimated coefficients A, N_0 and t are presented in Table 2 along with the estimated errors. Apparently N_0 is not a constant since more disks are required to reach percolation as the disk size is reduced. The exponent, t, however, is approximately a constant with an average value around 2.02.

Since the critical disk number N_0 is not an invariant, it is preferable to use the quantity η as defined previously in place of N in the approximate formula. Figure 2.16(a) thru (d) show the conductivity as a function of η for four different disk radii 0.05, 0.07, 0.1, and 0.15, respectively. The power law function should then be expressed in the modified form as follows:

$$K = \sigma_0(\eta - \eta_0)^t, \text{ for } \eta>\eta_0 \tag{2.24}$$

with the parameters tabulated in Table 3. The conductivity rapidly increases as η exceeds η_0. The same figures also show that the variation in the result increases with the radius. In fact the average standard deviation increases from 8.47×10^{-5} at r=0.05 to 1.80×10^{-4} at r=0.15, due to the reduced disk number for percolation.

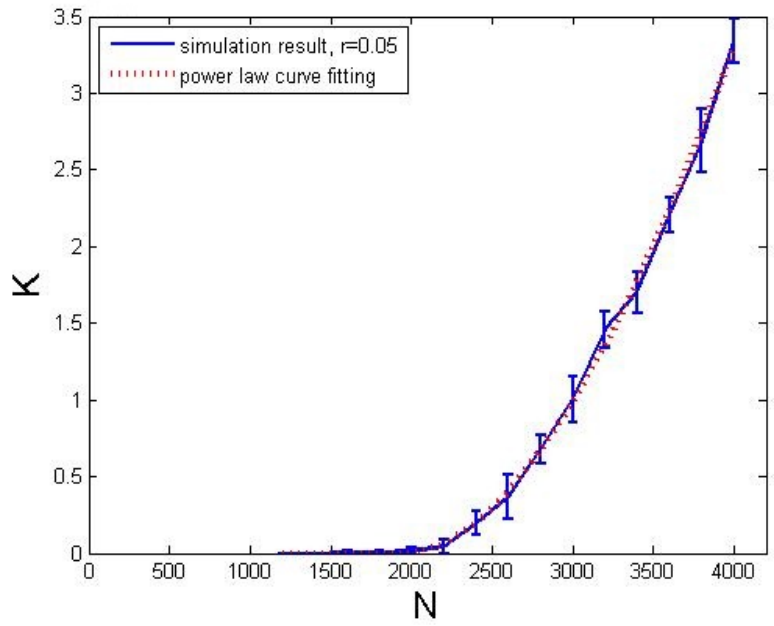

Figure 2.15 (a): Conductivity K as a function of fiber number for radius 0.05

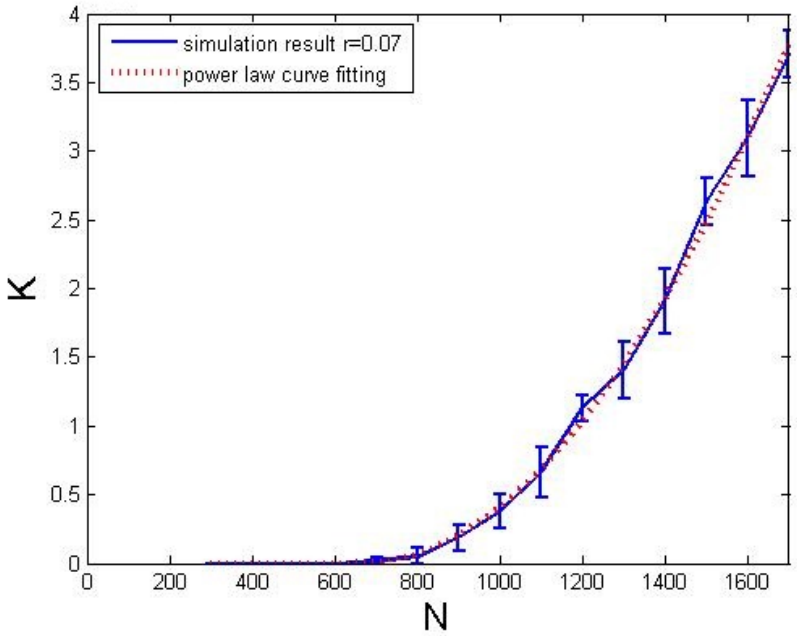

Figure 2.15 (b): Conductivity K as a function of fiber number for radius 0.07

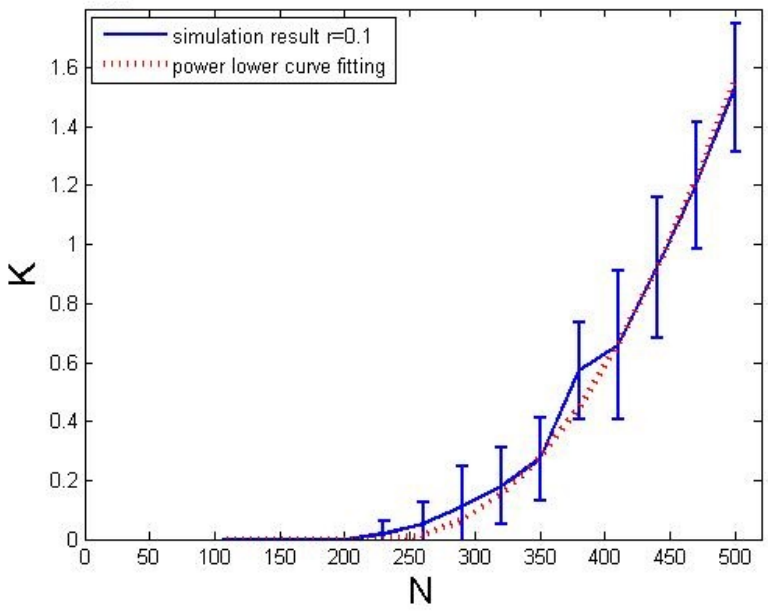

Figure 2.15 (c): Conductivity K as a function of fiber number for radius 0.10

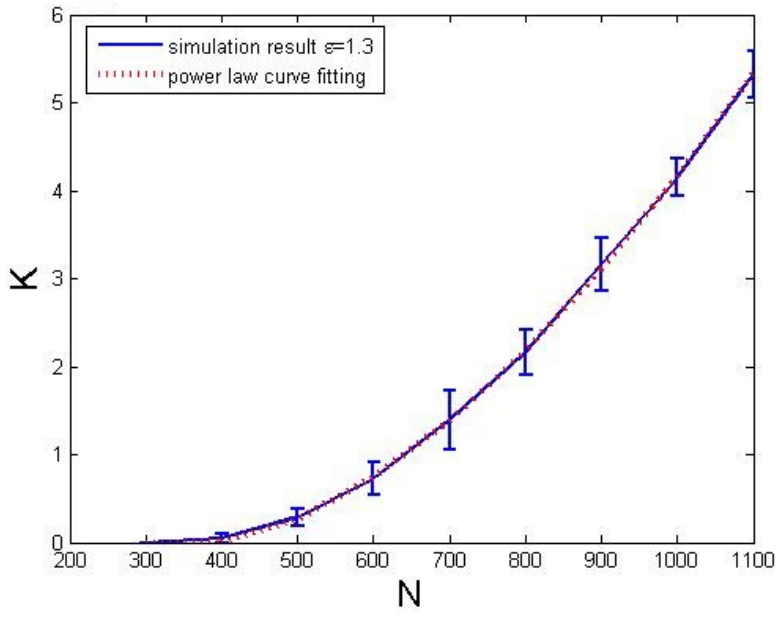

Figure 2.15 (d): Conductivity K as a function of fiber number for radius 0.15

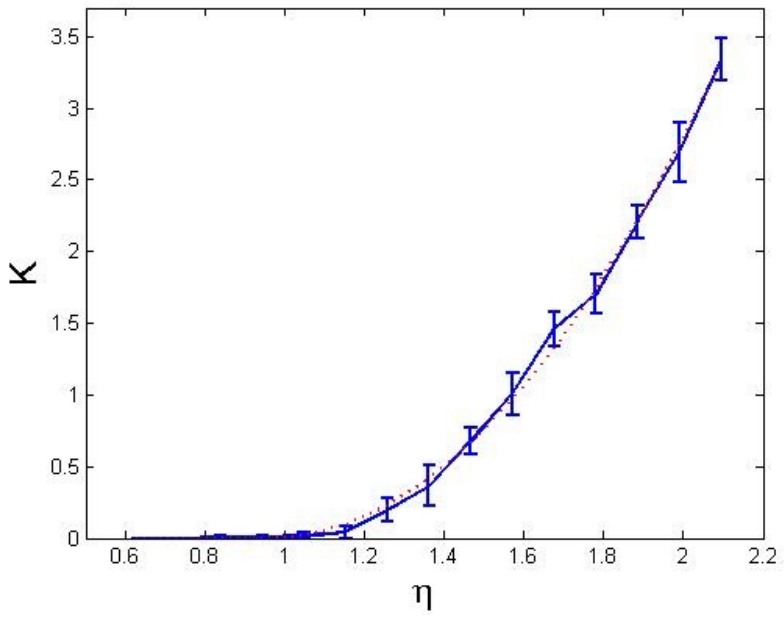

Figure 2.16 (a): Conductivity K as function of η for radius 0.05

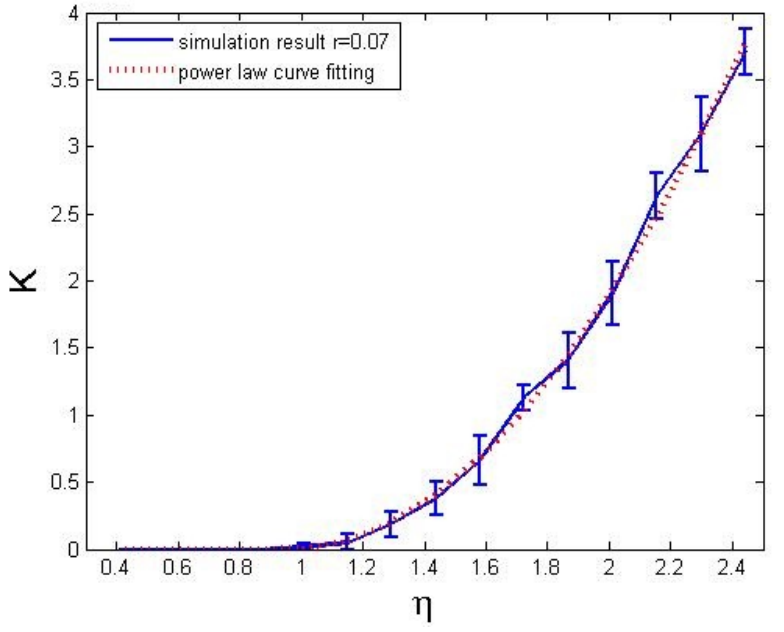

Figure 2.16 (b): Conductivity K as function of η for radius 0.07

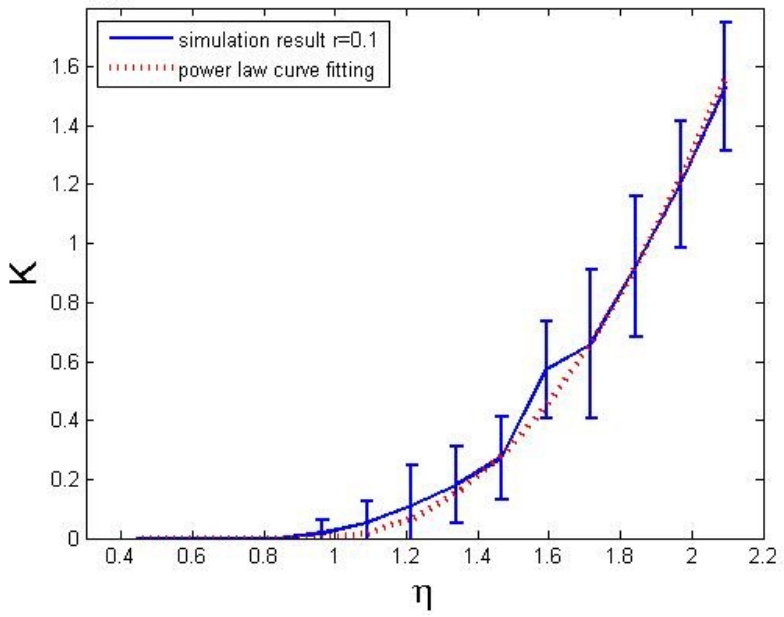

Figure 2.16 (c): Conductivity K as function of η for radius 0.10

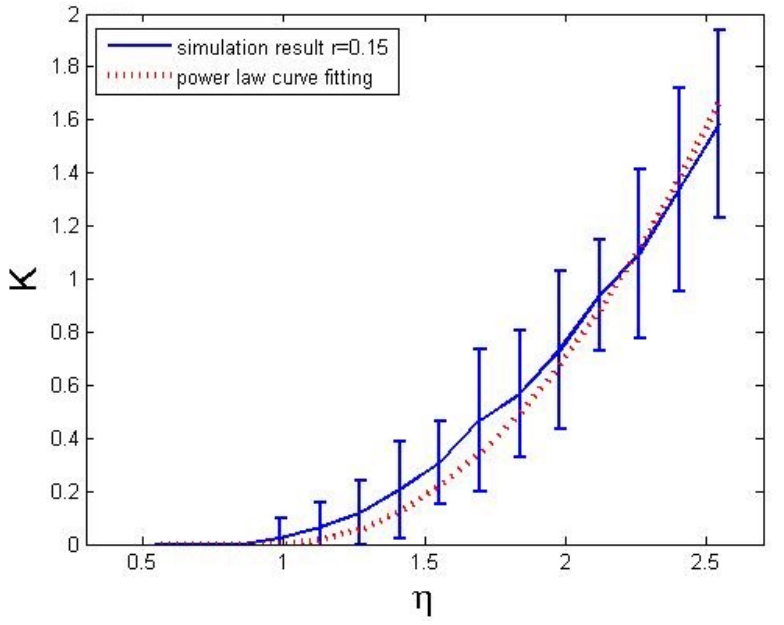

Figure 2.16 (d): Conductivity K as function of η for radius 0.15

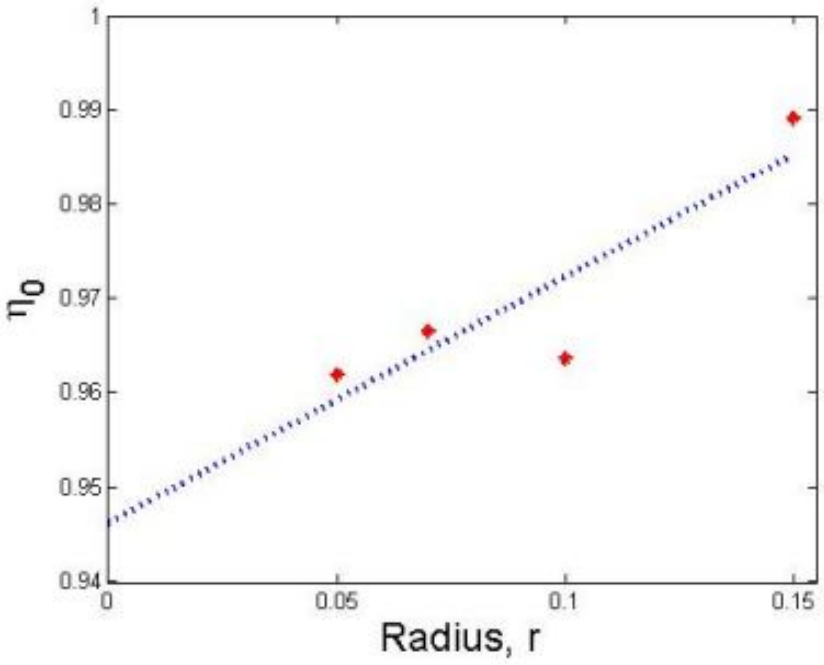

Figure 2.17: Determination of percolation threshold at r=0 using linear extrapolation

Table 2: Power-Law curve fitting results based on Eq. 2.18

Radius, r	***A***	***N_0***	***t***	**Squared 2-norm of residual**
0.05	7.2177×10^{-7}	1838.014	2.0000	1.8351×10^{-6}
0.07	5.1105×10^{-6}	673.199	1.9488	3.2237×10^{-6}
0.10	1.1106×10^{-5}	230.152	2.1177	6.2088×10^{-6}
0.15	1.3246×10^{-4}	70.001	2.0082	$1.487`\times10^{-6}$

Table 3: Power-law curve fitting results based on Eq. 2.20

Radius, r	σ_0	N_0	t	Squared 2-norm of residual
0.05	2.596	0.9624	2.0000	1.8351×10^{-6}
0.07	1.771	0.9672	1.9488	3.2237×10^{-6}
0.10	1.206	0.9641	2.1177	6.2088×10^{-6}
0.15	0.687	0.9896	2.0082	$1.487`\times10^{-6}$

2.5.3 Estimation of percolation threshold

As r approaches zero, N_0 approaches infinity for percolation. However, according to the percolation theory, η_0 approaches a constant value, which is defined as the percolation threshold of the system, η_c. We have observed a slight increase in η_0 as r increases. To estimate the percolation threshold we applied a linear extrapolation to find the intersection of η_0 at r=0, as shown in Fig. Based on the curve fitting, we estimated a solution of η_c=0.9462 $\pm$ 0.0001. This value of η_c is slightly lower than the solution reported previously [40], which is η_c=0.9614 $\pm$0.0006, with a difference around 1.6%. The underestimated result in the current study could be related to the finite element analysis, which is an approximate method, as well as the different number of disks used in the two distinct models. It should be noted that the previous study in the literature involved the detection of percolation paths based on geometric connectivity without using numerical approximations. Therefore it is not surprising to see the discrepancy in the two solutions. Nevertheless it is a good agreement in view of the order of magnitude

in the error. Generally speaking the solution obtained from the finite element analysis is less accurate since the matrix operations required in the finite element analysis cost substantially more computational effort.

The critical volume fraction of the disk in the system can be expressed by applying the equation that based on the percolation theory:

$$\phi_c = 1 - e^{-\eta_c} \tag{2.25}$$

where ϕ_c is the critical volume of the particles, η_c is the percolation threshold of the system. Following the equation, we can estimate the volume fraction of the disks in the system. The volume fraction of this study is approximately 62%. According to the previous review, this study has potential application in predicting the conductivity of graphene-based composite. We have found that the result is fairly close to the experimental result (67%) of grafted polypropylene (gPP)/expanded graphite (EG) nanocomposites via solution intercalation by Shen et al [62]. The difference between these two results is only 7.5%. Some reasons may cause the difference between our simulation result and the experimental result, such as the various polymer matrices and different aspect ratio of the GNP particles. However, the comparison with the experimental result confirms that our model and results can be applied in the composite materials, which contain the graphene-based material.

By applying a similar technique, we successfully obtained an approximate value $\sigma_0 \approx 4.64$ as r approaches zero. However, a logarithm function was used in the curve fitting due to the high nonlinearity in the relationship between r and σ_0. Therefore in the limiting case, the power-law function can be written in the following approximate form:

$$K = 4.64(\eta - 0.946)^{2.02}, r \to 0 \tag{2.26}$$

We also investigated the effect of the size distribution on the conductivity by introducing a binary sized distribution of disks of two different radii, r_1 and r_2, as shown in Fig. 2.18. We define the ratio of the two radii to be $\lambda=r_1/r_2$. Assume the two types of disks have the same number and we have f=0.5 where f represents the fraction of disks of radius r_1. We fixed the total disk number in this binary distribution while chose the value of r such that the corresponding η defined in Eq. (2.26) is maintained the same as that of the equi-sized disk system. If the equi-sized disks have radius r, then the relationship between r and r_1, r_2 can be found as

$$2r^3 = r_1^3 + r_2^3 \tag{2.27}$$

and thus

$$r_2 = r\left(\frac{2}{(1+\lambda^3)}\right)^{1/3}, \; r_1 = \lambda r_2 \tag{2.28}$$

Based on these assumptions, simulations can be performed in a fashion similar to the equisized disk system and the resulting percolation threshold; η_c can be evaluated as well. We set λ=2 and r=0.07, therefore,

$$r_1 = 0.08480, \; r_2 = 0.04240 \tag{2.29}$$

In addition to this work, we also investigated a binary mixture using the equivalent area instead of volume. This is driven by the fact that each individual disk is a two dimensional geometry. To do so, we considered

$$2r^2 = r_1^2 + r_2^2 \tag{2.30}$$

Setting λ=2 and r=0.07 leads to

$$r_1 = 0.08854,\ r_2 = 0.04427 \tag{2.31}$$

Table 4 shows the simulation results of percolation threshold for the two different types of binary mixture of disks. It has been found that η_c=0.9407 for the case using the cubic function, and η_c=0.8616 for the case using the square function. Compared to the result from the uniform dispersion, apparently the cubic function yields a much closer solution with a difference only about 0.6%. It is again confirmed that the statistical invariant for percolation of disks must be a cubic function of the characteristic length. The result also implies that one can use the average particle size in a polydisperse system to approximate the equivalent conductivity with a reasonably good accuracy if the variation in the particle size is not quite significant (e.g when 0.5<λ<2).

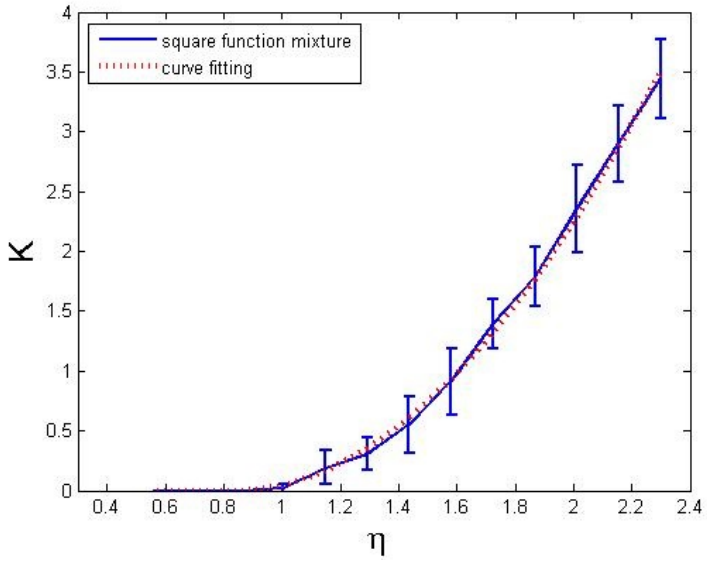

Figure 2.18 (a): Conductivity K as function of η for square function mixture, radius 0.07

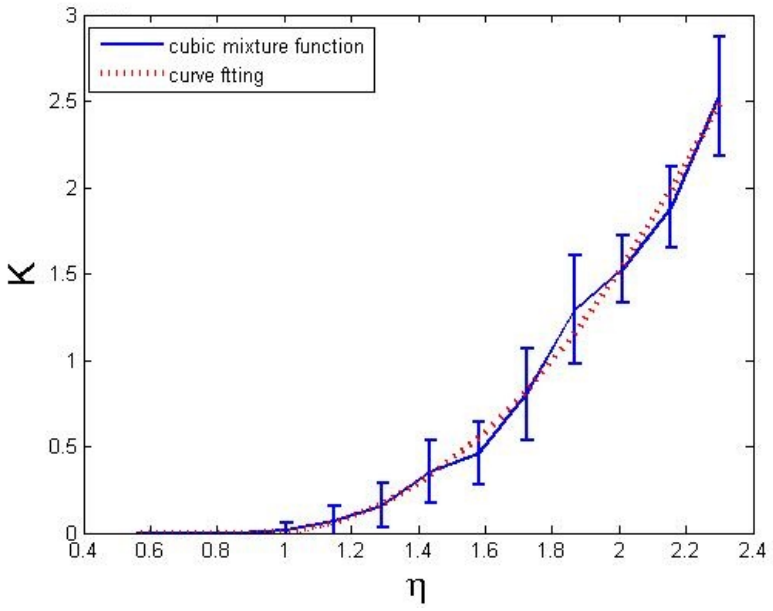

Figure 2.18(b): Conductivity K as function of η for square function mixture, radius 0.07

Table 4: Power-law curve fitting results based on Eq. 2.18

Type of mixing	σ_0	η_0	t	**Squared 2-norm of residual**
Cubic function	1.346	0.9407	2.0027	1.8472×10^{-6}
Square function	1.749	0.8616	1.9150	3.6280×10^{-6}

CHAPTER THREE: CONDUCTIVITIES AND PERCOLATION OF ELLIPTICAL PLATELETS

3.1 Simulation Method of Elliptical Platelets

3.1.1 Element generation and partition

Different from a circular disk, which has a constant curvature along the perimeter, the curvature and the tangential angle of an elliptical disk vary with the location.

$$\kappa(t) = \frac{ab}{(b^2 \cos^2 t + a^2 \sin^2 t)^{3/2}}, \tag{3.1}$$

$$\phi(t) = \tan^{-1}(\frac{a}{b}\tan t) \ . \tag{3.2}$$

In order to avoid excessive local elements and numerical inaccuracy induced by the local singularities of the solution, we have to modify the parameters including the curvature cutoff threshold and maximum element size. Figure 3.1 show the finite element meshes with different element densities generated by COMSOL©. As we can see, there is a high concentration of triangular elements at those locations of large curvature if the default values of the mesh generation parameters are used. To minimize the computational time, we reduced the number of elements significantly by adjusting the parameters such as the cutoff and minimum number of elements in the code. We use the same intersection

criteria and processes that we mentioned in the former chapter to analyze the ellipse system. Figures 3.2 (a) and (b) show a complete finite element model containing 1,000 elliptical plates with aspect ratio equal to 1.4. The semi-minor axis is 0.07, and approximately 200,000 elements by using the automated mesh generation scheme that we used in the disk-shaped particles.

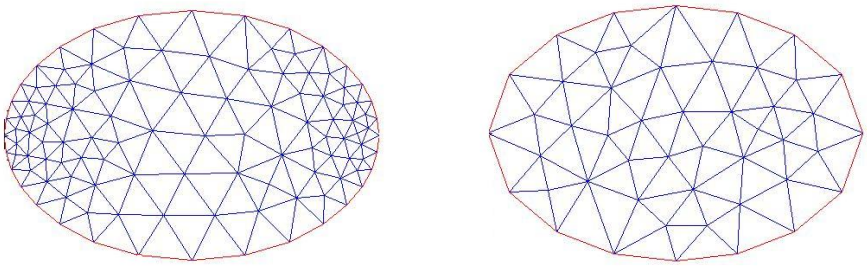

Figure 3.1: shows the COMSOL© generated elliptical platelets with aspect ratio 1.5: (a) a fine mesh generated using the default values of mesh generation parameters; (b) a coarse mesh generated using the adjusted values of mesh generation parameters.

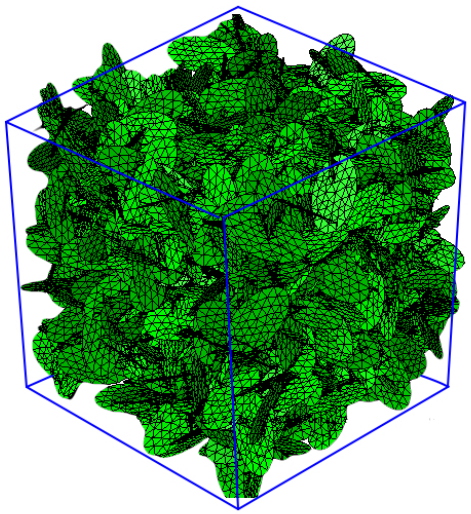

Figure 3.2 (a): A complete finite element mesh for the entire model with 1000 elliptical platelets with aspect ratio 1.4 and approximately 20000 elements in the unit.

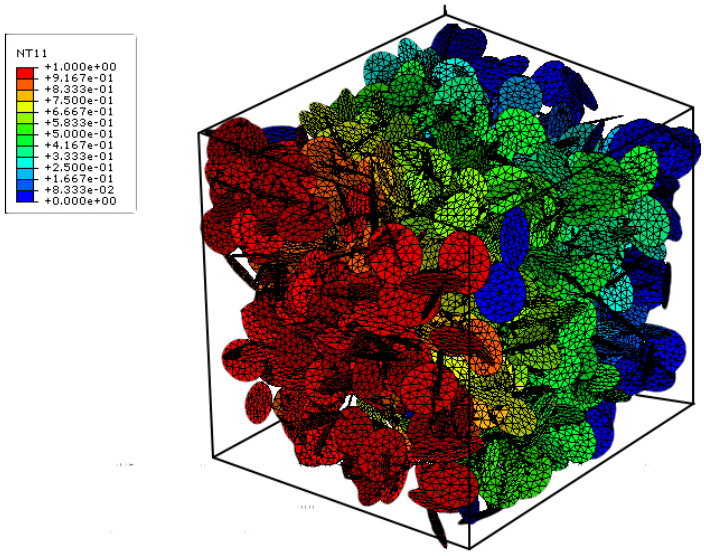

Figure 3.2 (b): Finite element simulation of the entire model with 1000 elliptical plates, aspect ratio 1.1 and approximately 15000 elements in a unit cell. A unit temperature gradient is applied on the opposite sides of the cell.

We varied the aspect ratio of the ellipses from 1.1 to 1.5 in our study. The semi-minor axis of each situation is equal to 0.07. The smallest ellipse size nearly corresponds to one-sixth of the unit cell and the largest size is approximately one-fifth of the unit cell. The simulations were run around 10 times at each volume fraction (or equivalently, each number of ellipses) depending on the size of radius. The results were collected and the means and the standard deviations were computed afterwards.

3.1.2 Percolation threshold of elliptical platelets

The definition of the percolation threshold for elliptical platelets should be consistent with that of the equivalent three-dimensional system rather than planar systems. According to the previous chapter, we define the following variable to measure the percolation threshold for thin elliptical plates:

$$\eta = \frac{4}{3} N \pi R^3 \ , \tag{3.3}$$

and

$$A_0 = \pi R^2 = \pi ab, \tag{3.4}$$

where R is the equivalent radius; a and b are the semi-axis lengths of ellipse; N is the plate number per unit volume; A_0 is the area of ellipse. Combining the former two equations, we can define the percolation threshold of elliptical plates as follows:

$$\eta = \frac{4}{3} \pi a b^2 N \ . \tag{3.5}$$

3.1.3 Curve-fitting method for elliptical particles

The curve-fitting method is the same as the one used in the previous study. Through the approximation, we determine the lower bounds of N_0 at certain values are 500, 400, 300, 200, 100, when the aspect ratio is equal to 1.1, 1.2, 1.3, 1.4 and 1.5, respectively. The upper bounds of N_0 are 700, 500, 400, 300 and 200, respectively. The lower and

upper bounds of conductivity exponent, t, are 1 and 3. For the coefficient A, the value ranges from 10^{-4} to 10^{-8}.

3.2 Simulation Results for the Elliptical Platelets

By using the same curve fitting method, coefficients A, N_0 and t are presented in Table 5 along with the estimated errors. Obviously, N_0 is not a constant since more plates are required to reach percolation as the disk size is reduced. The exponent, t, is not considered in this research, since the elliptical shape is a more complex geometry compared to circular disks, which may affect t. The exponent, t, is not a constant in elliptical plates with different aspect ratios. We will discuss the exponent, t, in the future work. In the table, the variation in the result increases with the aspect ratio. In fact the average standard deviation increases from 1.8472×10^{-6} at ε=1.1 to 5.6244×10^{-10} at ε=1.5. Shown in Figure 3.3 (a) through (e) are the simulation results of the equivalent conductivity expressed as a function of the elliptical plate number for five different radii ranging from 1.1 to 1.5. The semi-minor axis of those plates is 0.07. The total number of elliptical platelets varies from 500 to 200 accordingly. To evaluate the statistical variations, the simulations were repeated 10 times for each aspect ratio. The curve in each plot in Figure 3.3 is similar to the result of disk-shaped particle. The conductivity remains zero until the particle number reaches a critical value that is equivalent to the percolation threshold. The conductivity is nonlinearly related to the plate number. Using the Eq.3.5 can approximate the simulation results. Figure 3.4 (a) thru (e) show the conductivity as a function of η for five aspect ratios with the same semi-major axis. The aspect ratios are

1.1, 1.2, 1.3, 1.4 and 1.5 respectively. By using the same Eq. 3.5, we tabulate our results in Table 3. As we mentioned before, in order to reduce the computational time, we choose the less element density model in our study. Although by reducing the element density on the plate can help us to save more computational time, the precision of the result decreased. We compared the simulation results with aspect ratio ε equal to 1.5 for both low and high element density model in our study. The result shows that the percolation threshold η_c equal to 0.6231 by using the fine element mesh generation scheme. However, the percolation threshold η_c decreased to 0.5310 with a difference of 17.3% when using the coarse mesh generation scheme. Obviously, to study the effect of the aspect ratio on the conductivity, we need to use a finer mesh generation scheme. Due to the limitation of the computer capability, we will use a finer mesh generation scheme in the future.

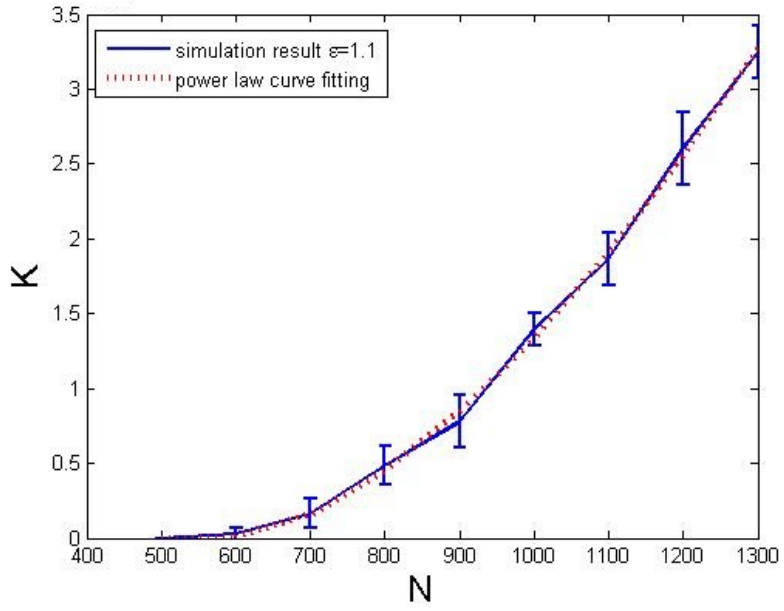

Figure 3.3(a): Conductivity K as a function of elliptical plate number for ε=1.1

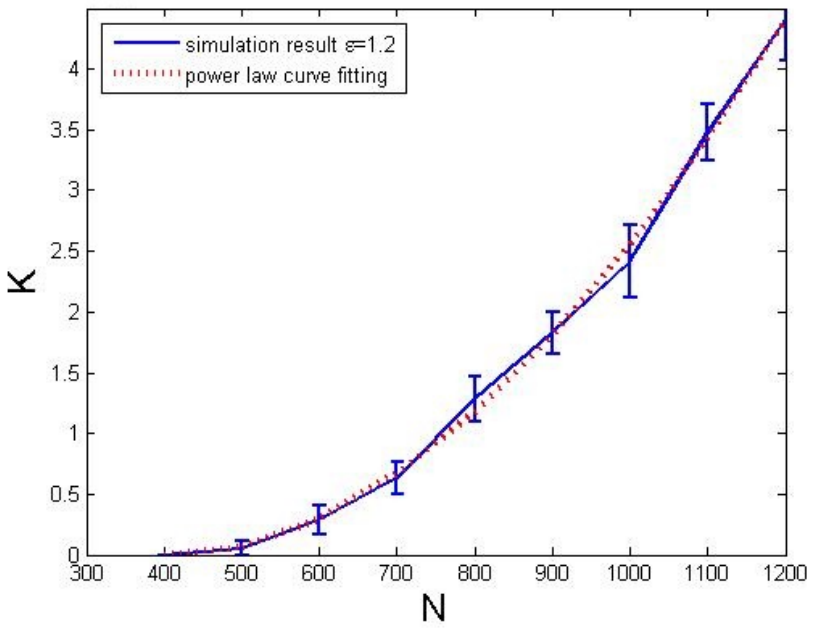

Figure 3.3(b): Conductivity K as function of elliptical fiber number for ε=1.2

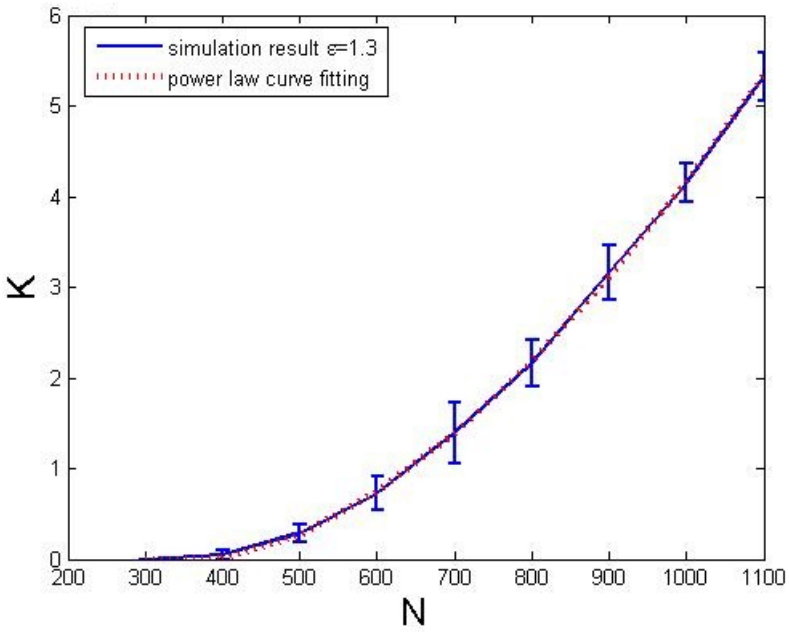

Figure 3.3(c): Conductivity K as a function of elliptical plate number for ε=1.3

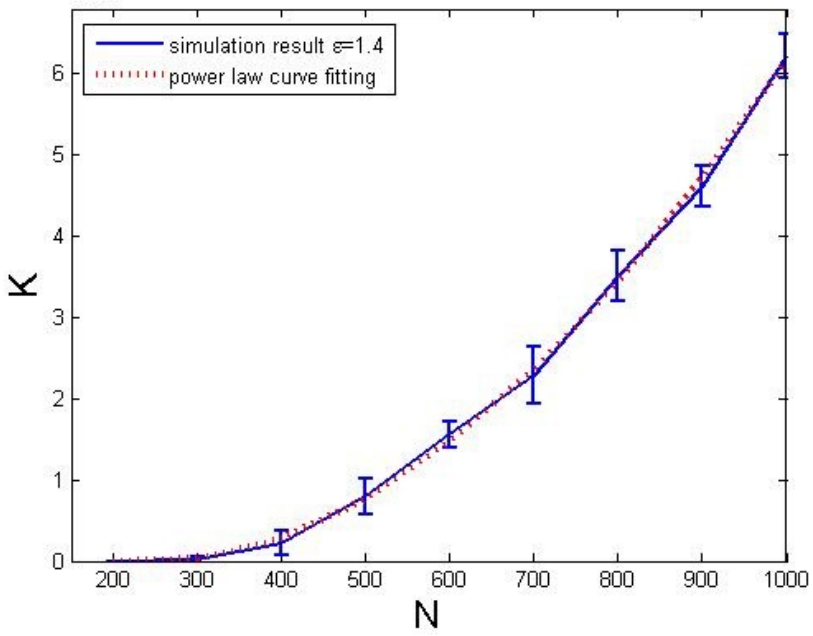

Figure 3.3(d): Conductivity K as function of elliptical fiber number for ε=1.4

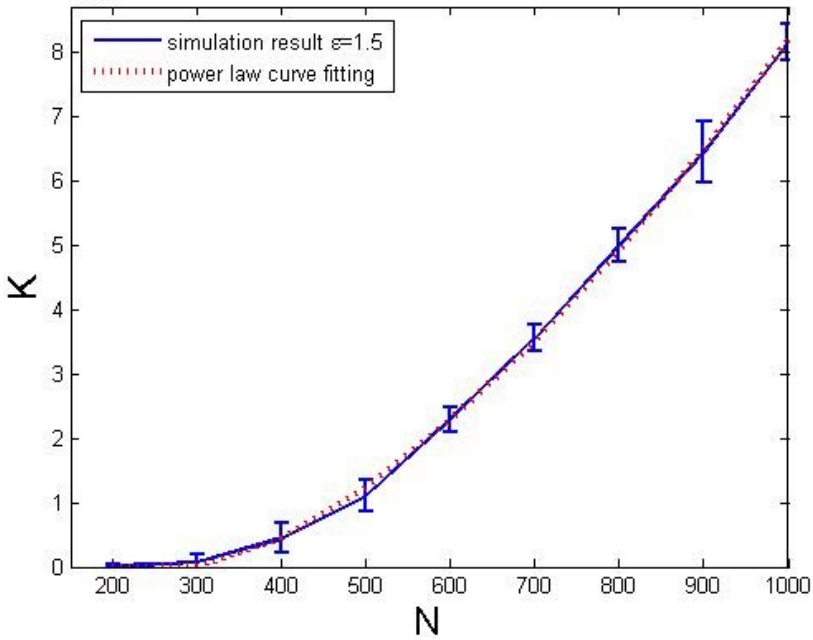

Figure 3.3(e): Conductivity K as a function of elliptical plate number for ε=1.5

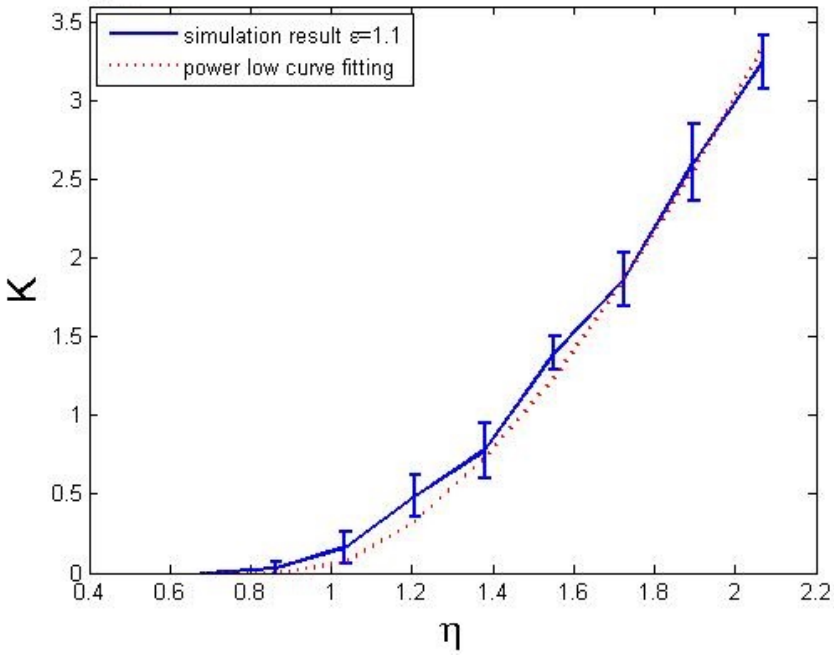

Figure 3.4(a): Conductivity K as a function of η defined in Eq. 3.5 for ε=1.1.

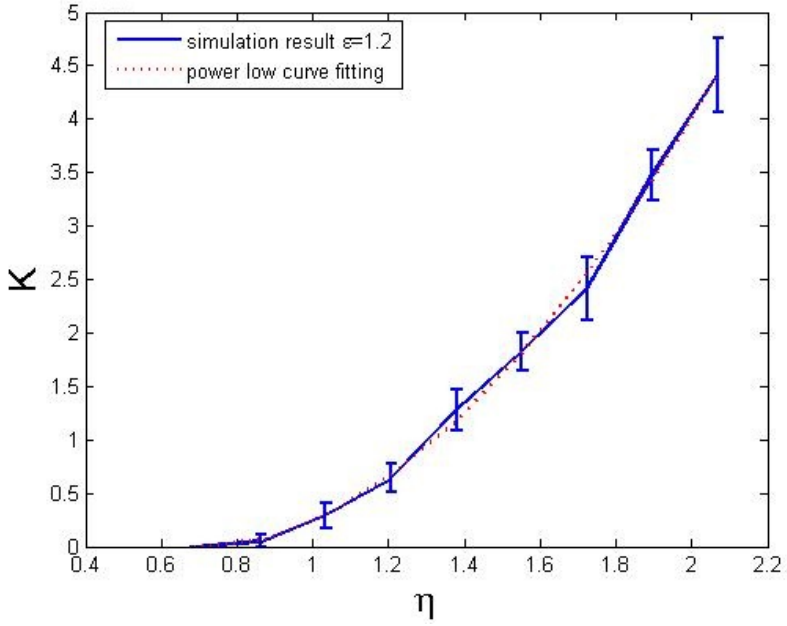

Figure 3.4(b): Conductivity K as a function of η defined in Eq. 3.5 for ε=1.2.

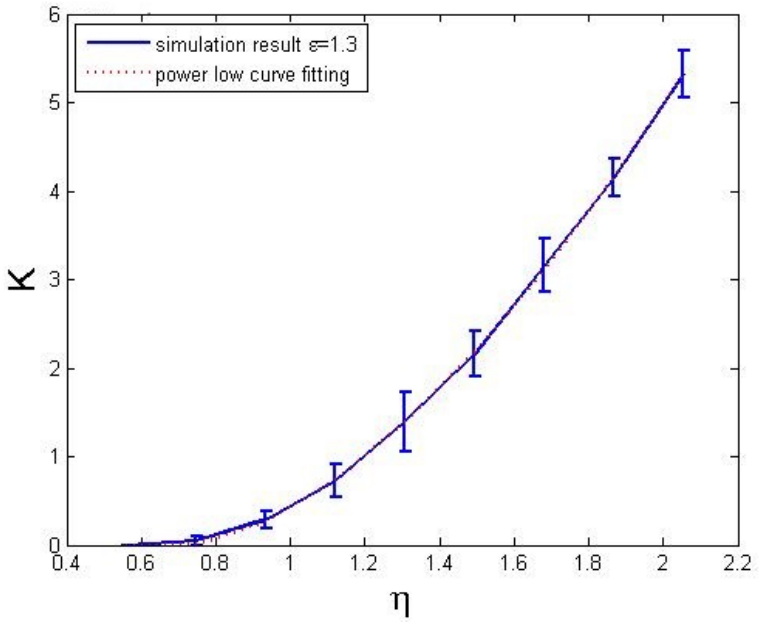

Figure 3.4(c): Conductivity K as a function of η defined in Eq. 3.5 for ε=1.3.

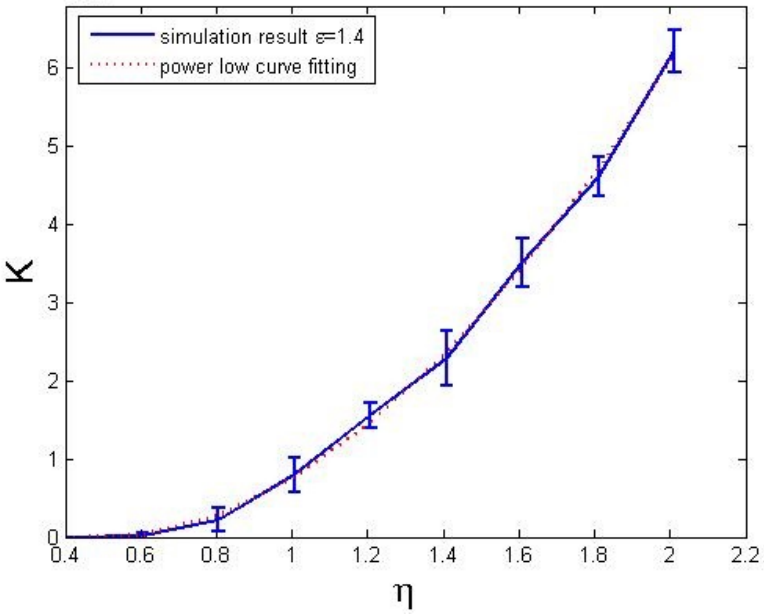

Figure 3.4(d): Conductivity K as a function of η defined in Eq. 3.5 for ε=1.4.

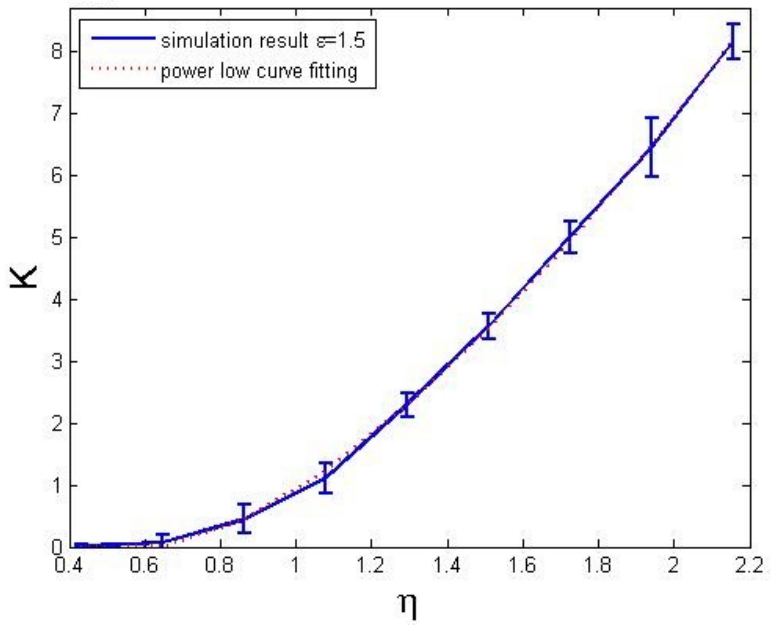

Figure 3.4(e): Conductivity K as a function of η defined in Eq. 3.5 for ε=1.5.

Table 5: Power-law curve fitting results based on Eq. 2.18

Aspect ratio	**A_0**	**N_0**	***t***	**squared 2-norm of the residual**
1.1	7.3397E-08	589.5741	1.6304	1.8472E-06
1.2	2.2655E-08	422.1079	1.8295	3.6280E-06
1.3	1.2377E-07	389.9029	1.6252	3.9971E-06
1.4	3.4579E-08	263.9634	1.8316	4.4217E-06
1.5	3.9549E-07	298.0743	1.5160	5.6244E-06

Table 6: Power-law curve fitting results based on Eq. 3.5

Aspect Ratio, ε	σ_0	η_0	t	Squared 2-norm of residual
1.1	4.640	0.9318	1.6304	1.8472×10^{-6}
1.2	6.630	0.7283	1.8295	3.6280×10^{-6}
1.3	1.310	0.7278	1.6252	3.9971×10^{-6}
1.4	1.835	0.6424	1.8316	4.4217×10^{-6}
1.5	1.720	0.5310	1.5160	5.6244×10^{-6}

Fig. 3.5 shows η_c plotted against the aspect ratio $\boldsymbol{\varepsilon}$**.** According to the figure, percolation threshold rapidly decreases as the aspect ratio ε increases. In fact, η decreases by 0.4 from 0.9318 to 0.5310. The figure shows the higher aspect ratio the lower percolation threshold in the system. We have not considered the critical exponent t in this situation; however, we can estimate that the critical exponent is smaller than 2 that is lower than the exponent for circular platelets. According to the figure, we believe that aspect ratio strongly affects the percolation threshold. It should be pointed out that the results are noticeably lower than that reported by Yi (2009), although in his research the results also shows that higher aspect ratio ε_0 will lead to a reduction in the percolation threshold η_0. The reason behind this discrepancy is yet unknown. However, there are several factors that may cause our results lower than the former studies. First one is that we introduced the finite element method into this research and the former studies just focused on the traditional probabilistic simulation. The different methods used may have

led to different results, especial for the elliptical platelets that have geometric effects on the percolation threshold. Secondly, since we applied the finite element method in our study, the element size in each unit cannot be too small; otherwise it would cost extensive computational effort. However, with large platelets, the scaling effect can be non-negligible. In addition, each elliptical platelet contains more nodes and elements, and therefore the computation is more intensive in each simulation. This imposes a limitation on the trial number that we can use in the simulations. To save the computational time, we have to reduce the number of plates. For instance, in Yi's research without using the finite element method the model has over ten thousand plates, whereas in our studies the maximum number of plates can only reach a few hundred to a few thousand. In other words, we are unable to obtain enough data for predicting the results. This may lead to a significant inaccuracy in the result. Due to above reasons, it is not surprising to see the discrepancy in the comparison here.

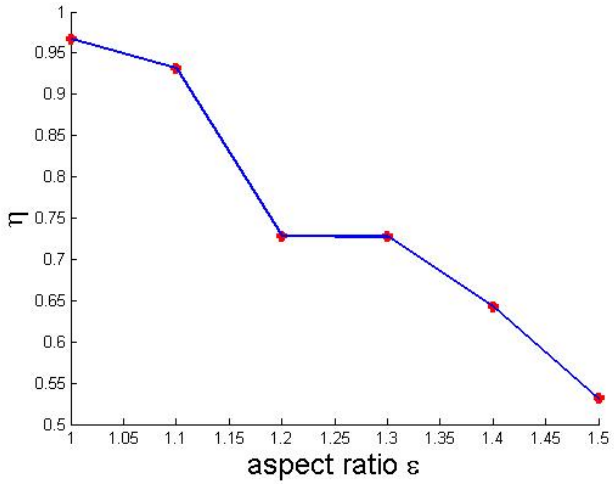

Figure 3.5: The percolation threshold η_c as a function of aspect ratios $\boldsymbol{\varepsilon}$.

CHAPTER FOUR: CONCLUSIONS AND FUTURE WORK

4.1 Conclusions

The effective conductivities of randomly positioned and oriented circular platelets are determined by using an efficient computational algorithm based on the Monte Carlo modeling and the finite element method. The disks are discretized using a specialized element partition scheme to construct a continuous mesh that consists of interconnected shell elements. The equivalent conductivity is computed from the reactive flux in a simulation cell subjected to a unit potential across the domain. The computational algorithms are optimized to accommodate particles of different sizes and to minimize the computational time. It has been found that the results can be fitted into a power-law function and the key parameters in the function have been determined from the curve fitting techniques. The estimated percolation threshold is in the close vicinity of the prior results reported in the literature, where a different solution method was used. It has also been confirmed that the definition of percolation threshold is consistent with that of the equivalent particulate system in three dimensions. In addition, the thickness significantly affects the conductivity of the system; high thickness of the particles will increase the conductivity of the whole system. For a binary sized distribution of disks with half of the disks having radii twice as large as the others, it has been found that the concept using the equivalent volume yields more accurate results compared to the equivalent area, and

therefore the statistical invariant is indeed a cubic function of the characteristic size of the system.

For the elliptical plates, the same computational algorithm based on the Monte Carlo modeling and the finite element method is used. The plates are discretized using the same element partition scheme with reasonable parameters in order to generate interconnected triangular shell elements. The equivalent conductivity is computed for five different aspect ratio systems. The computational algorithms and schemes are optimized to accommodate particles of different sizes and to minimize the computational time. According to the simulation results, the electrical and thermal conductivities of filled polymer composites are strongly dependent on the aspect ratio of the filler. High aspect ratio will decrease the percolation threshold. Much lower percolation thresholds can be achieved for the elliptical plates in our simulations compared to the results reported in the literature. Several reasonable explanations are proposed.

Due to the analogy between electrical and thermal conductions, the dimensionless results reported here can be interpreted as either electrical conductivity or thermal conductivity. The methods and results in this study are useful in predicting conduction and percolation of both monodisperse and polydisperse materials that contain disk-shaped particles, and have potential applications in predicting the material properties of graphene platelets. In addition, the results of the elliptical plates demonstrated that the material properties of particulate composites are closely linked to the aspect ratio and surface-to-volume ratio of the filler. The research findings from this work can be applied to graphene-sheet-based composites that have extremely high aspect ratios. The low percolation threshold for three-dimensional isotropic structure of graphene-based

composites is evident due to the extremely large aspect ratio of the graphene sheets and their excellent homogeneous dispersion in the matrix. In order to significantly improve the conductivity of particulate composites, filler contents of high aspect ratio are preferred. The limitation of the current study lies in the assumption that the disks are fully overlapping. Future studies will involve partially penetrable disks that may reflect more realistic conditions.

4.2 Future Work

In order to improve the accuracy of the computational results, we propose several different approaches in future. In our methodology, we developed an automated mesh generation scheme with COMSOL©. Although this method is quite convenient and efficient, a finer mesh is required to obtain sufficiently accurate solutions, especially for studying material systems consisting of inclusions of different sizes and aspect ratios. In the future, depending on the geometric morphologies of particles, we need to develop different mesh generation schemes. In addition, more powerful computational tools will be used to make the simulations more efficient. We have proposed several reasons to explain the inaccuracy in our current models for the elliptical plates; one of the most major obstacles lies in the inability of the current method to discretize a sufficiently large number of plates simultaneously. In addition, a more suitable approach can be used to model percolation in disk-shaped particulate systems. One of the most promising methods is hard-core/soft-shell model in which each conducting inclusion is modeled as an impenetrable hard core surrounded by a soft shell. In this model, the hard core

represents the actual inclusion (filler) and the soft shell represents the related tunneling distance. The hard-core/soft-shell model has been already widely used to investigate the model of micro-emulsions and liquid in which spherical particles are considered [52], [53], [54]. Van den Berg and Steif showed the hard-core model as a simple model of a gas whose particles have non-negligible size. [58] The hard-core/soft-shell model is also used in nanotube composites. Figure 5.1 shows that a nantotube is treated as a hard-core model with a soft shell. Several researchers already proved that the hard-core representation is more appropriate for modeling composite materials due to the existence of tunneling in the main charge transport mechanism [54], [55].

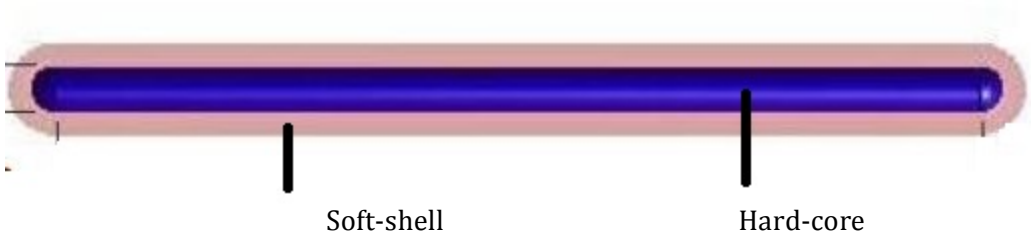

Figure 4.1 Hard-core model with a soft shell of radius for CNT.

For the disk-shaped platelets, we may also use hard-core/soft-core model. Here, we propose a simple model for the disk-shaped particles dispersed in a randomly system to accommodate a hard disk core and a soft shell. Considering a system of randomly dispersed system, it is natural to associate a hard-core radius r_b and a penetrable shell, r_a-r_b, with each disk plate. We call r_a-r_b as the "percolation distance" [58]. We can assume two disks are connected if the distance between their centers is less than 2a, however, this distance is not allowed to be less than 2b. Therefore, the formation of a connected network of particles via such overlaps is a percolation problem in which the connectivity

and the corresponding geometrical and physical properties are expected to be dependent on the ratio *b/a*. The exact values of *a* and *b* depend on the realistic, experimental data. The percolation threshold occurs when a system-spanning cluster forms at a unique value of the percolation distance. Apparently, the thermodynamic interaction between the soft shell and the hard core is not considered in this model. Monte Carlo simulation will be used, and the mesh of the elements can be generated by the finite element method. As we mentioned before, the particle clustering and percolation have been used to explain a wide range of macroscopic phenomena including the conductivity of conducting particles randomly embedded in a non-conducting matrix. Therefore, we will be able to make predictions on the thermal and electrical conductivities by using this model. Meanwhile, we can also investigate the effect of parameters such as the fiber type and the molecular weight of the polymer matrix on the tunneling distance in polymer nanocomposites. Figure 4.2 shows the hard-core/soft-core model of the disk-shaped particulate system. The red spot shown in the figure is hard-disk core; the yellow one is the soft shell; *a* is the radius of disk; and *b* is the radius of hard disk.

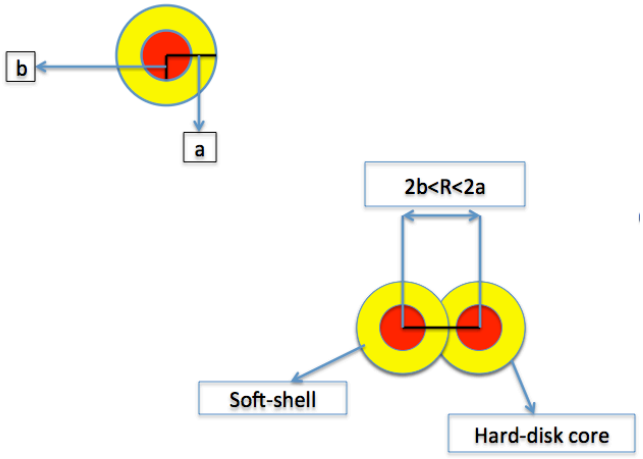

Figure 4.2: Hard-core disks with soft shells in a 3-D particulate system.

REFERENCES

1. Geim, Andre K., and Konstantin S. Novoselov. "The rise of graphene." *Nature materials* 6.3 (2007): 183-191.

2. Stankovich, Sasha, et al. "Graphene-based composite materials." *Nature*442.7100 (2006): 282-286.

3. Geim, Andre Konstantin. "Graphene: status and prospects." *science* 324.5934 (2009): 1530-1534.

4. Pumera, Martin. "Graphene-based nanomaterials and their electrochemistry." *Chemical Society Reviews* 39.11 (2010): 4146-4157.

5. Yu, Aiping, et al. "Graphite nanoplatelet-epoxy composite thermal interface materials." *The Journal of Physical Chemistry C* 111.21 (2007): 7565-7569.

6. Prolongo, S. G., et al. "Graphene nanoplatelets thickness and lateral size influence on the morphology and behavior of epoxy composites." *European Polymer Journal* (2014).

7. King, Julia A., et al. "Mechanical properties of graphene nanoplatelet/epoxy composites." *Journal of Applied Polymer Science* 128.6 (2013): 4217-4223.

8. Gao, Jiefeng, et al. "Graphite-Nanoplatelet-Decorated Polymer Nanofiber with Improved Thermal, Electrical, and Mechanical Properties." *ACS applied materials & interfaces* 5.16 (2013): 7758-7764.

9. Novoselov, Kostya S., et al. "Electric field effect in atomically thin carbon films."*science* 306.5696 (2004): 666-669.

10. Zhang, T., and Y. B. Yi. "Monte Carlo simulations of effective electrical conductivity in short-fiber composites." *Journal of applied physics* 103.1 (2008): 014910.

11. Rosowsky, André. "An analytical method to compute an approximate value of the site percolation threshold pc." *The European Physical Journal B-Condensed Matter and Complex Systems* 15.1 (2000): 77-86.

12. Seaton, N. A., and Eduardo D. Glandt. "Monte Carlo simulation of adhesive disks." *The Journal of chemical physics* 84.8 (1986): 4595-4601.

13. Binder, Kurt, and Dieter W. Heermann. *Monte Carlo simulation in statistical physics: an introduction*. Springer, 2010.

14. McGreevy, R. L., and L. Pusztai. "Reverse Monte Carlo simulation: a new technique for the determination of disordered structures." *Molecular Simulation*1.6 (1988): 359-367.

15. Nayak, Rajlakshmi, Dora P. Tarkes, and Alok Satapathy. "A computational and experimental investigation on thermal conductivity of particle reinforced epoxy composites." *Computational Materials Science* 48.3 (2010): 576-581.

16. Hasselman, D. P. H., and Lloyd F. Johnson. "Effective thermal conductivity of composites with interfacial thermal barrier resistance." *Journal of Composite Materials* 21.6 (1987): 508-515.

17. Douglas, Jr, Jim, and Thomas F. Russell. "Numerical methods for convection-dominated diffusion problems based on combining the method of characteristics with finite element or finite difference procedures." *SIAM Journal on Numerical Analysis* 19.5 (1982): 871-885.

18. Shimada, Kenji, and David C. Gossard. "Automatic triangular mesh generation of trimmed parametric surfaces for finite element analysis." *Computer Aided Geometric Design* 15.3 (1998): 199-222.

19. Flory, Paul J. "Molecular size distribution in three dimensional polymers. I. Gelation1." *Journal of the American Chemical Society* 63.11 (1941): 3083-3090.

20. Hammersley, John Michael. "Percolation processes. Lower bounds for the critical probability." *Ann. Math. Statist* 28.790-795 (1957): 2.

21. Balberg, I., and N. Binenbaum. "Cluster structure and conductivity of three-dimensional continuum systems." *Physical Review A* 31.2 (1985): 1222.

22. Berkowitz, B., and I. Balberg. "Percolation approach to the problem of hydraulic conductivity in porous media." *Transport in Porous Media* 9.3 (1992): 275-286.

23. Li, Jing, and Jang-Kyo Kim. "Percolation threshold of conducting polymer composites containing 3D randomly distributed graphite nanoplatelets." *Composites science and technology* 67.10 (2007): 2114-2120.

24. Bollobas, Bela, and Oliver Riordan. *Percolation*. Cambridge University Press, 2006.

25. Meester, Ronald. *Continuum percolation*. No. 119. Cambridge University Press, 1996.

26. Balberg, I. "Recent developments in continuum percolation." *Philosophical Magazine Part B* 56.6 (1987): 991-1003.

27. Lorenz, Christian D., and Robert M. Ziff. "Precise determination of the critical percolation threshold for the three-dimensional “Swiss cheese” model using a growth algorithm." *The Journal of Chemical Physics* 114.8 (2001): 3659-3661.

28. Yi, Y. B. "Void percolation and conduction of overlapping ellipsoids." *Physical Review E* 74.3 (2006): 031112.

29. Kirkpatrick, Scott. "Percolation and conduction." *Reviews of modern physics*45.4 (1973): 574.

30. Tawerghi, Elyas, and Yun-Bo Yi. "A computational study on the effective properties of heterogeneous random media containing particulate inclusions."*Journal of Physics D: Applied Physics* 42.17 (2009): 175409.

31. Balberg, I., and N. Binenbaum. "Computer study of the percolation threshold in a two-dimensional anisotropic system of conducting sticks." *Physical Review B*28.7 (1983): 3799.

32. Balberg, I., N. Binenbaum, and N. Wagner. "Percolation thresholds in the three-dimensional sticks system." *Physical Review Letters* 52.17 (1984): 1465.

33. Foygel, M., et al. "Theoretical and computational studies of carbon nanotube composites and suspensions: Electrical and thermal conductivity." *Physical Review B* 71.10 (2005): 104201.

34. Grujicic, M., G. Cao, and W. N. Roy. "A computational analysis of the percolation threshold and the electrical conductivity of carbon nanotubes filled polymeric materials." *Journal of materials science* 39.14 (2004): 4441-4449.

35. Kertesz, J. "Percolation of holes between overlapping spheres: Monte Carlo calculation of the critical volume fraction." *Journal de Physique Lettres* 42.17 (1981): 393-395.

36. Elam, W. T., A. R. Kerstein, and J. J. Rehr. "Critical properties of the void percolation problem for spheres." *Physical review letters* 52.17 (1984): 1516.

37. Rintoul, MARK DANIEL. "Precise determination of the void percolation threshold for two distributions of overlapping spheres." *Physical Review E* 62.1 (2000): 68.

38. Van der Marck, S. C. "Network approach to void percolation in a pack of unequal spheres." *Physical review letters* 77.9 (1996): 1785.

39. Yi, Y. B., and K. Esmail. "Computational measurement of void percolation thresholds of oblate particles and thin plate composites." *Journal of Applied Physics* 111.12 (2012): 124903.

40. Yi, Y. B., and E. Tawerghi. "Geometric percolation thresholds of interpenetrating plates in three-dimensional space." *Physical Review E* 79.4 (2009): 041134.

41. 41. Mertens, Stephan, and Cristopher Moore. "Continuum percolation thresholds in two dimensions." *Physical Review E* 86.6 (2012): 061109.

42. Quintanilla, J., S. Torquato, and Robert M. Ziff. "Efficient measurement of the percolation threshold for fully penetrable discs." *Journal of Physics A: Mathematical and General* 33.42 (2000): L399.

43. Douglas, Jr, Jim, and Thomas F. Russell. "Numerical methods for convection-dominated diffusion problems based on combining the method of characteristics with finite element or finite difference procedures." *SIAM Journal on Numerical Analysis* 19.5 (1982): 871-885.

44. Douglas, Jr, Jim, and Thomas F. Russell. "Numerical methods for convection-dominated diffusion problems based on combining the method of characteristics with finite element or finite difference procedures." *SIAM Journal on Numerical Analysis* 19.5 (1982): 871-885.

45. Cai, Wen-Zhong, Shan-Tung Tu, and Guo-Liang Tao. "Thermal conductivity of PTFE composites with three-dimensional randomly distributed fillers." *Journal of Thermoplastic Composite Materials* 18.3 (2005): 241-253.

46. Quintanilla, J. "Measurement of the percolation threshold for fully penetrable disks of different radii." *Physical Review E* 63.6 (2001): 061108.

47. Quintanilla, John A., and Robert M. Ziff. "Asymmetry in the percolation thresholds of fully penetrable disks with two different radii." *Physical Review E*76.5 (2007): 051115.

48. Consiglio, R., et al. "Continuum percolation thresholds for mixtures of spheres of different sizes." *Physica A: Statistical Mechanics and its Applications* 319 (2003): 49-55.

49. Yi, Y-B., and A. M. Sastry. "Analytical approximation of the percolation threshold for overlapping ellipsoids of revolution." *Proceedings of the Royal Society of London. Series A: Mathematical, Physical and Engineering Sciences*460.2048 (2004): 2353-2380.

50. Version, ABAQUS Standard User'S. Manual. "6.9, 2009. Pawtucket, RI: Hibbit, Karlsson & Sorensen."

51. Manual, Comsol. "Comsol multiphysic user's guide." (2005).

52. Berhan, L., and A. M. Sastry. "Modeling percolation in high-aspect-ratio fiber systems. I. Soft-core versus hard-core models." *Physical Review E* 75.4 (2007): 041120.

53. Van den Berg, J., and J. E. Steif. "Percolation and the hard-core lattice gas model." *Stochastic Processes and their Applications* 49.2 (1994): 179-197.

54. Balberg, I., and N. Binenbaum. "Invariant properties of the percolation thresholds in the soft-core–hard-core transition." *Physical Review A* 35.12 (1987): 5174.

55. Hu, Chin-Kun, and Kit-Sing Mak. "Percolation and phase transitions of hard-core particles on lattices: Monte Carlo approach." *Physical Review B* 39.4 (1989): 2948.

56. Baker, Don R., et al. "Continuum percolation threshold for interpenetrating squares and cubes." *Physical Review E* 66.4 (2002): 046136.

57. Rintoul, M. D., and S. Torquato. "Precise determination of the critical threshold and exponents in a three-dimensional continuum percolation model." *Journal of Physics A: Mathematical and General* 30.16 (1997): L585.

58. Heyes, David M., Michael Cass, and Arkadiusz C. Brańka. "Percolation threshold of hard-sphere fluids in between the soft-core and hard-core limits."*Molecular Physics* 104.20-21 (2006): 3137-3146.

59. Deng, Fei, and Quan-Shui Zheng. "An analytical model of effective electrical conductivity of carbon nanotube composites." *Applied Physics Letters* 92.7 (2008): 071902.

60. Kim Christensen. *Percolation Theory*. MIT, Oct. 2002. Web. 5 Jun. 2014.

61. Wilkinson, David, and Jorge F. Willemsen. " Invasion percolation: a new form of percolation theory." *Journal of Physics* A: *Mathematical and General* 16.14 (1983): 3365.

62. Chen, Xiao-Mei, Jing-Wei Shen, and Wen-Yi Huang. "Novel electrically conductive polypropylene/graphite nanocomposites." *Journal of materials science letters* 21.3 (2002): 213-214.